

Sub-seasonal forecasting with a large ensemble of deep-learning weather prediction models

Jonathan A. Weyn^{1*}, Dale R. Durran¹, Rich Caruana², Nathaniel Cresswell-Clay¹

¹Department of Atmospheric Sciences, University of Washington

²Microsoft Research, Redmond, Washington

Key Points:

- An ensemble forecast system is developed using convolution neural networks (CNNs) to generate data-driven global forecasts.
- Only 3 seconds are required to compute a large 320-member ensemble of skillful 6-week sub-seasonal predictions.
- Shorter lead time forecasts also show skill, including a single deterministic 4-day forecast for Hurricane Irma.

*Current affiliation: Microsoft, Redmond, WA, USA.

Corresponding author: J. Weyn, jweyn@uw.edu

Abstract

We present an ensemble prediction system using a Deep Learning Weather Prediction (DLWP) model that recursively predicts key atmospheric variables with six-hour time resolution. This model uses convolutional neural networks (CNNs) on a cubed sphere grid to produce global forecasts. The approach is computationally efficient, requiring just three minutes on a single GPU to produce a 320-member set of six-week forecasts at 1.4° resolution. Ensemble spread is primarily produced by randomizing the CNN training process to create a set of 32 DLWP models with slightly different learned weights.

Although our DLWP model does not forecast precipitation, it does forecast total column water vapor, and it gives a reasonable 4.5-day deterministic forecast of Hurricane Irma. In addition to simulating mid-latitude weather systems, it spontaneously generates tropical cyclones in a one-year free-running simulation. Averaged globally and over a two-year test set, the ensemble mean RMSE retains skill relative to climatology beyond two-weeks, with anomaly correlation coefficients remaining above 0.6 through six days.

Our primary application is to subseasonal-to-seasonal (S2S) forecasting at lead times from two to six weeks. Current forecast systems have low skill in predicting one- or 2-week-average weather patterns at S2S time scales. The continuous ranked probability score (CRPS) and the ranked probability skill score (RPSS) show that the DLWP ensemble is only modestly inferior in performance to the European Centre for Medium Range Weather Forecasts (ECMWF) S2S ensemble over land at lead times of 4 and 5-6 weeks. At shorter lead times, the ECMWF ensemble performs better than DLWP.

Plain Language Summary

We develop a machine learning weather prediction system, trained on past weather data, thereby providing an alternative approach to the current widely used computer models that predict the weather based on approximate mathematical representations of physical laws. Our approach is much more computationally efficient, allowing us to make a very large number of similar forecasts, known as an ensemble, for the same weather event. The ensemble better defines the range of possible future weather conditions than a single forecast. Our ensembles show skill at both short forecast lead times and for 4-6-week (sub-seasonal) prediction. The sub-seasonal predictions are for 1 or 2-week averaged weather patterns. Although our forecasts are better than benchmark guesses, such as a forecast consisting of the average weather conditions on a given calendar date, the quantitative forecast skill remains low for sub-seasonal prediction. Nevertheless, by several quantitative measures our forecasts at 4-6 weeks score nearly as well as the current state-of-the-art forecasts from major operational centers. The ease with which our machine learning approach can efficiently generate very large ensemble forecasts holds promise for future developments to improve the skill of sub-seasonal prediction.

1 Introduction

Weather forecasting relies heavily on data assimilation to estimate the current state of the atmosphere and on numerical weather prediction (NWP) to approximate its subsequent evolution. The skill of such deterministic weather forecasts is typically limited to about two weeks by the chaotic growth of small initial errors and inaccuracies in our approximate models of the atmosphere. On much longer, multi-month time scales, the coupling of the atmosphere with slowly evolving ocean-land forcing allows skillful seasonal forecasts of monthly or seasonally averaged conditions. Between these two extremes, the production of skillful one- or two-week averaged forecasts at lead times ranging roughly between two weeks and two months (the so-called subseasonal-to-seasonal or S2S time frame) has proved particularly challenging; yet there are many societal sectors that would

63 greatly benefit from improved S2S forecasts (White et al., 2017). Several major oper-
 64 ational centers have developed NWP-based ensemble systems focused on improving S2S
 65 forecasting (Vitart et al., 2017).

66 In 1992, the European Centre for Medium-Range Weather Forecasts (ECMWF)
 67 and the National Centers for Environmental Prediction (NCEP) began issuing ensem-
 68 ble weather forecasts. They were soon followed by the other major weather prediction
 69 centers across the world. Ensemble forecasts strive to provide a set of equally-likely fore-
 70 cast realizations spanning the range of possible future atmospheric states. Early evidence
 71 for the economic value of probabilistic forecasts derived from the ECMWF ensemble rela-
 72 tive to a single deterministic forecast was provided by Richardson (2000). Ensemble fore-
 73 casts are now recognized as essential to represent the probabilistic nature of weather fore-
 74 casting and to break through the intrinsic limits to predictability of the atmosphere (Palmer,
 75 2018).

76 Ensembles are particularly appropriate as one looks beyond lead times where de-
 77 terministic forecasts lose all skill relative to climatology. On S2S lead times, ensemble-
 78 mean and ensemble-based probabilistic forecasts have shown modest skill relative to cli-
 79 matology (Vitart, 2004; Weigel et al., 2008; Vitart, 2014; Monhart et al., 2018). Com-
 80 putational resources do, however, impose a significant limitation on efforts to create S2S
 81 forecasts with NWP ensembles. As of 2016, 11 forecast centers were contributing S2S
 82 forecasts to the S2S database (Vitart et al., 2017), and the ensembles from three of these
 83 centers consisted of just four members. The largest S2S ensemble, with 51 members pro-
 84 viding forecasts out to 46 days, is generated by ECMWF’s Integrated Forecast System
 85 (IFS) using a significant fraction of the time available on one of the world’s most pow-
 86 erful computer systems (Bauer et al., 2015). Yet there is increasing evidence that the
 87 number of ensemble members for S2S forecasts should be higher, perhaps in the 100-200
 88 range (Buizza, 2019). Large ensemble sizes are also helpful for assessing the likelihood
 89 of events in the tails of probabilistic forecast distributions (Leutbecher, 2018), and such
 90 extreme events are often the most impactful.

91 Machine learning provides one potential avenue to develop S2S forecasts systems
 92 with significantly lower computational costs. Recognizing that there are other success-
 93 ful machine-learning approaches to S2S forecasting (Hwang et al., 2019), here our focus
 94 will be on the development of a data-driven deep-learning weather prediction (DLWP)
 95 model that can be iteratively stepped forward, like traditional NWP models, to simu-
 96 late atmospheric states at arbitrarily long lead times. In one of the first attempts to use
 97 ML to create such a model, Dueben and Bauer (2018) trained neural networks (NNs)
 98 on several years of reanalysis data to predict 500 hPa geopotential height (Z_{500}) on the
 99 globe at 6° resolution, demonstrating the ability to produce ML weather forecasts that
 100 have at least modest forecast skill. Using advanced convolutional neural networks (CNNs),
 101 Scher and Messori (2019) trained algorithms on simulations from a simplified GCM that
 102 significantly outperformed baseline metrics and effectively captured the simplified-GCM
 103 dynamics at spherical harmonic resolutions of T21 and T42 (roughly 5.6° and 2.8°). Train-
 104 ing only on historical data, Weyn et al. (2019) used CNNs to generate forecasts for north-
 105 ern mid-latitude Z_{500} and 300-700-hPa thickness ($\tau_{300-700}$) on a 2.5° latitude-longitude
 106 grid that showed skill relative to climatology and persistence through five days.

107 Recently we extended our DLWP model to the full globe using a volume-conservative
 108 mapping to project global data from latitude-longitude grids onto a cubed sphere and
 109 improved the CNN architecture operating on the cube faces (Weyn et al., 2020, here-
 110 after WDC20). In addition to Z_{500} and $\tau_{300-700}$, our improved model forecasts two ad-
 111 ditional surface fields, 1000 hPa height (Z_{1000}) and 2-meter temperature (T_2), and uses
 112 three externally-specified 2D fields: a land-sea mask, topographic height, and top of the
 113 atmosphere insolation. This new 1.9° resolution model showed skill relative to climatol-
 114 ogy and persistence through seven days. Moreover, it could be stepped forward repeat-

115 edly from a single initialization for at least one year, and while doing so, captured the
 116 seasonal cycle with reasonable accuracy.

117 In the following we further improve our DLWP model by adding two more 2D prog-
 118 nostic fields and increasing the spatial resolution to 1.4° . Large 320-member ensembles
 119 generated using the improved model are used to provide S2S forecasts through a six-week
 120 lead time. These forecasts are verified against ERA5 data and compared to operational
 121 ECMWF S2S products.

122 The remainder of this paper is organized as follows. Section 2 describes the improve-
 123 ments to our previous DLWP model, while section 3 discusses the incorporation of that
 124 model in our ensemble forecast system. The behavior of that ensemble is assessed at short
 125 deterministic lead times in section 4, and at longer S2S lead times in section 5. Section
 126 6 contains the conclusions.

127 2 The DLWP model

128 The basic model is very similar to that described in detail in WDC20, in which four
 129 forecast fields, geopotential height at 1000 hPa (Z_{1000}) and at 500 hPa (Z_{500}), 300-700
 130 hPa thickness ($\tau_{300-700}$), and 2-meter temperature (T_2), are mapped to a cubed sphere.
 131 Three known fields are also provided: top-of-atmosphere radiation, topographic height,
 132 and a land-sea mask. Convolutional neural networks (CNN) were trained using the same
 133 3×3 set of horizontal spatial filters on all four equatorial faces on the cube (WDC20, Fig. 1).
 134 A different set of filters was applied to the two polar faces. A U-Net architecture (Ronneberger
 135 et al., 2015) with skip connections is employed to capture multi-scale processes via av-
 136 erage pooling and corresponding up-sampling. The skip connections across each level of
 137 spatial refinement ensure high-resolution information is preserved. The activation func-
 138 tions are leaky ReLU functions capped at a scaled value of 10. The model is recursively
 139 stepped forward with 12-hr time steps, such that a single step maps the fields at two time
 140 levels $t_0 - 6$ and t_0 hr to forecast fields at $t_0 + 6$ and $t_0 + 12$ hr. The model is trained
 141 to minimize the mean squared error (MSE) over two steps, or equivalently over a 24-hr
 142 period with 6-hr temporal resolution.

143 Here we extend the WDC20 model by adding two more forecast fields: tempera-
 144 ture at 850 hPa (T_{850}), which is strongly modulated by large-scale weather patterns while
 145 exhibiting less sensitivity to diurnal heating and surface-layer processes than T_2 , and to-
 146 tal column water vapor (TCWV). TCWV is the vertically-integrated total gas-phase wa-
 147 ter above each grid cell; its inclusion is a step toward characterizing tropical convective
 148 systems including tropical cyclones and the Madden-Julian oscillation (MJO). The MJO
 149 is believed to be an important source of forecast skill on S2S time scales and has been
 150 characterized as a “moisture mode” (Adames & Kim, 2016).

151 The resolution was also modestly increased from 48×48 to 64×64 grid cells on
 152 each face of the cube, yielding an effective resolution of approximately 1.4° in latitude
 153 and longitude at the equator. ERA5 data at a gridded resolution of 1° in latitude and
 154 longitude were remapped with the Tempest-Remap package (Ullrich & Taylor, 2015; Ull-
 155 rich et al., 2016) for training, validation and testing. Somewhat fortuitously, the WDC20
 156 convolutional neural network architecture continued to perform quite well despite the
 157 changes to the model input and target data, although we were able to improve the model
 158 by doubling the number of filters used in each convolutional layer. This increased the
 159 number of filters in the first layer from 32 to 64. Our improved DLWP CNN architec-
 160 ture is tabulated in Table 1. The increases in the number of filters in each layer and num-
 161 ber of forecast fields increased the total number of trainable parameters relative to that
 162 in WDC20 by about a factor of about 4, to 2.7 million. Nevertheless, as a result of ad-
 163 ditional code optimization, the model still trains in 6–8 days.

Table 1. CNN architecture for DLWP as a sequence of operations on layers. The parameter v represents the number of input fields, t represents the number of input time steps, and c represents the number of auxiliary prescribed inputs (here top-of-atmosphere radiation at t times, land-sea mask and topographic height). The layer names (except for the suffix “CubeSphere”) correspond to the names in the Keras Library. “Concatenate” appends the state in parentheses, numbered earlier, to the output of the previous layer.

Layer	Filters	Filter size	Output shape ^a	Trainable params ^b
<i>input</i>			(6, 64, 64, $vt + c$)	
Conv2D–CubeSphere	64	3×3	(6, 64, 64, 64)	18,560
Conv2D–CubeSphere (1)	64	3×3	(6, 64, 64, 64)	73,856
AveragePooling2D		2×2	(6, 32, 32, 64)	
Conv2D–CubeSphere	128	3×3	(6, 32, 32, 128)	147,712
Conv2D–CubeSphere (2)	128	3×3	(6, 32, 32, 128)	295,168
AveragePooling2D		2×2	(6, 16, 16, 128)	
Conv2D–CubeSphere	256	3×3	(6, 16, 16, 256)	590,336
Conv2D–CubeSphere	128	3×3	(6, 16, 16, 128)	590,080
UpSampling2D		2×2	(6, 32, 32, 128)	
Concatenate (2)			(6, 32, 32, 256)	
Conv2D–CubeSphere	128	3×3	(6, 32, 32, 128)	590,080
Conv2D–CubeSphere	64	3×3	(6, 32, 32, 64)	147,584
UpSampling2D		2×2	(6, 64, 64, 64)	
Concatenate (1)			(6, 64, 64, 128)	
Conv2D–CubeSphere	64	3×3	(6, 64, 64, 64)	147,584
Conv2D–CubeSphere	64	3×3	(6, 64, 64, 64)	73,856
Conv2D–CubeSphere	vt	1×1	(6, 64, 64, vt)	1,560

^aOutput shape is (face, y , x , channels).

^bNumber of learned parameters for $t = 2$, $v = 6$, $c = 4$. Total is 2,676,376.

3 Designing an ensemble of DLWP models

The basic ensemble design follows the typical practice used in operational NWP forecasting by including ensemble members with both perturbed initial conditions (ICs) and variations in the model’s representation of the atmosphere—the later being incorporated in NWP ensembles either through the use of several different “physics” parameterization packages, through a suite of different parameter values with a fixed set of packages, or through the incorporation of stochastic physics. The perturbed initial conditions and our approach to varying the model representation of the atmosphere are discussed below.

3.1 Initial condition uncertainty

The ERA5 dataset includes 10 perturbed ensemble members generated by ensemble data assimilation with 4DVAR (Isaksen et al., 2010) to help with uncertainty estimation, and we use these as a convenient set of perturbed ICs for construction of our DLWP ensemble. Unfortunately, this set of ICs is non-optimal, because, unlike the operational ECMWF ensemble (Palmer, 2018), singular vectors were not used to select the most rapidly growing initial perturbations. Moreover, the ERA5 ensemble itself is moderately under-dispersive (<https://confluence.ecmwf.int/display/CKB/ERA5%3A+uncertainty+estimation>).

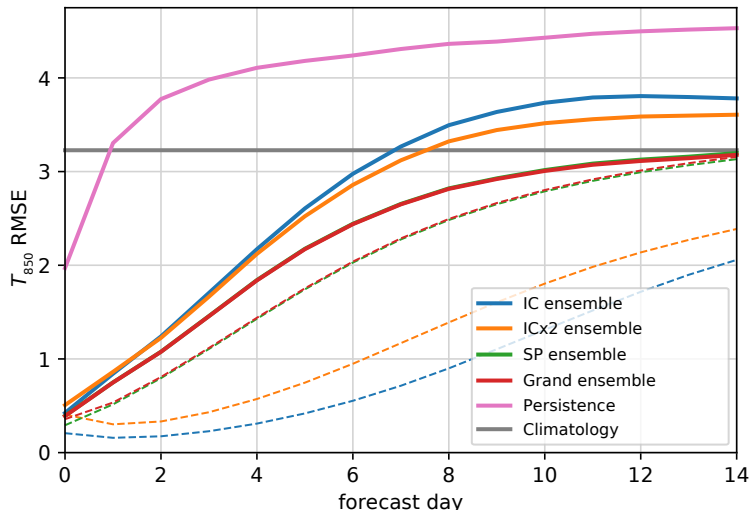


Figure 1. RMSE in T_{850} (K) as a function of forecast lead time for DLWP ensembles (solid lines) and corresponding ensemble spread (dashed): IC (blue), IC \times 2 (orange), stochastically perturbed (SP green) and the grand ensemble (red). Curves for the SP and grand ensemble are almost identical. Also shown are the RMSE for persistence (pink) and climatology (gray) benchmarks.

181 Figure 1 shows the globally-averaged RMSE of the ensemble mean T_{850} plotted as
 182 a function of forecast lead time for four DLWP ensemble strategies. Also plotted are RMSE
 183 reference curves for climatology and persistence. The solid blue curve shows the RMSE
 184 of a DLWP forecast generated using the 10 perturbed members of the ERA5 dataset to
 185 create a 10-member IC ensemble. Since the ERA5 IC perturbations do not project strongly
 186 on to the most rapidly growing modes, the ensemble spread (computed as the square root
 187 of the average over all forecasts of the ensemble variance) actually decreases over the first
 188 36 h of forecast lead time (dashed blue line in Fig. 1). In a conventional NWP model,
 189 such a reduction in ensemble spread, which occurs primarily on small spatial scales, can
 190 arise from a combination of numerical dissipation and the dispersion of inertia-gravity
 191 waves, and an analogous behavior is present in the DLWP model.

192 Another serious problem with the IC ensemble is that the spread is much smaller
 193 than the RMSE of the ensemble mean. In an ideal ensemble, the joint distribution of the
 194 ensemble members would be unchanged if the verifying observations were substituted
 195 for any one of the individual ensemble members, and under that assumption the spread
 196 and RMSE curves should coincide (Fortin et al., 2014). In an effort to better match the
 197 ensemble spread to the RMSE, a 10-member “IC \times 2” ensemble was created, in which the
 198 difference in the IC perturbations from the control ERA5 data was doubled. The spread
 199 for the IC \times 2 ensemble is modestly improved, and over the period 5–14 days the RMSE
 200 is modestly reduced (orange curves) relative to the original IC ensemble. Note that the
 201 reduction in initial ensemble spread over the first 36 h is more rapid in the IC \times 2 ensem-
 202 ble, providing further evidence that the variations in these initial condition do not strongly
 203 project on the structure of the most rapidly growing perturbations.

204 3.2 Uncertainty in the representation of the atmosphere

205 The learnable weights for convolutions in the CNN are initialized as small random
 206 values, and we can exploit this randomness by repeatedly retraining with different ini-

207 tial seeds to produce a family of DLWP models with slightly different final weights. The
 208 models in this family are capable of making approximately equally-skillful forecasts, but
 209 with enough statistical independence to produce a good ensemble. Scher and Messori
 210 (2020) pursued a similar strategy, training and re-training models to both emulate a sim-
 211 ple GCM and to forecast the real atmosphere with data from ERA5.

212 As part of its holistic estimation of the next atmospheric state, our CNN based DLWP
 213 model effectively captures physical processes that are parameterized in operational NWP
 214 models. For example, as noted in WDC20 (see also Fig. 5c,d), our DLWP model does
 215 an excellent job of forecasting 2-m temperatures, including their diurnal cycle, without
 216 using any explicit parameterization of boundary layer processes, and without including
 217 most of the meteorological fields that would be used in such parameterizations. We there-
 218 fore refer to the ensembles in which the CNN filter coefficients are randomly perturbed
 219 during training as “stochastically perturbed” (SP) ensembles, although the nature of the
 220 induced stochastic variations differs from that in operational NWP.

221 Rather than completely retrain each member of our SP ensemble from new ran-
 222 dom seeds, we gained efficiency by using intermediate results produced during the train-
 223 ing process. Our DLWP model is trained using the adaptive learning scheme Adam (Kingma
 224 & Ba, 2014). Figure 2 shows the learning curve for our loss function (mean squared er-
 225 ror, see WDC20) as a function of the training epoch number for a training cycle repre-
 226 sentative of that for one of our DLWP ensemble members. As expected, the error on the
 227 training set decreases smoothly, while the error on the validation set oscillates much more,
 228 strongly suggesting the learned weights in the model undergo nontrivial changes over each
 229 training epoch. The variations induced by these changes in the weights turn out to be
 230 sufficient to provide many useful members in a SP ensemble, and we exploited these vari-
 231 ations as follows.

232 After at least 100 training epochs, we selected multiple potential ensemble mem-
 233 bers from a single training cycle by checkpointing every 10 epochs and saving the model’s
 234 weights at each checkpoint. Using these checkpointed weights, we tested each resulting
 235 model’s utility for S2S forecasts by evaluating its average global T_{850} anomaly correla-
 236 tion coefficient (ACC) score at 4-week lead time from twice-a-week forecasts over the full
 237 four-year validation set. The 4-week T_{850} ACC scores for the checkpointed models were
 238 often equally good (or occasionally even better) than that for final trained model, and
 239 there was nearly as much ensemble spread between the various checkpoints of one train-
 240 ing cycle as there was between models generated by separate training cycles. (Although
 241 the final trained model had the lowest validation set loss during training, the training
 242 loss function is based solely on the RMSE over the first 24 hours of forecast lead time;
 243 it does not depend on the performance of a 4-week forecast.)

244 Our SP ensemble used a total of 32 slightly different DLWP models generated by
 245 eight training cycles with four members drawn from each cycle. The members selected
 246 from each cycle had the best 4-week T_{850} ACC scores, although three of the 32 mem-
 247 bers selected in this fashion required further refinement because in a few individual fore-
 248 casts they produced fields with unrealistic structures even though their numerical val-
 249 ues remained bounded within reasonable limits. Those three members were further train-
 250 ed for two more epochs using a re-initialized stochastic gradient descent (SGD) opti-
 251 mizer, which consistently fixed the issue with nonphysical solutions. The SGD cycles also
 252 lowered the training and validation loss slightly, as exemplified over the last 15 epochs
 253 of the learning curve in Fig. 2.

254 The RMSE and spread of the SP ensemble is plotted in Fig. 1. It clearly outper-
 255 forms the IC and IC \times 2 ensembles, having lower RMSE and a much better RMSE-spread
 256 relationship. The spread is roughly 80% of RMSE at a forecast lead time of 8 d and ap-
 257 proaches 95% by 14 d. At 14 d, the RMSE of the SP ensemble remains slightly better
 258 than climatology, whereas the RMSE for the IC and IC \times 2 ensembles begins to exceed

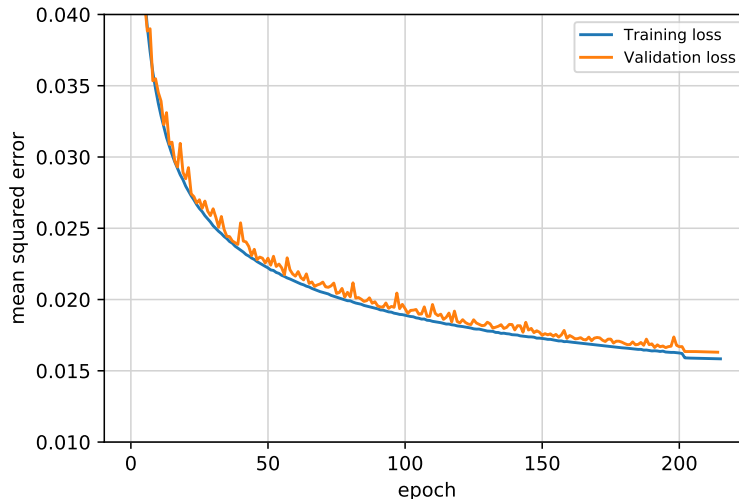


Figure 2. Example of the CNN learning curve for a representative DLWP model. The loss, which is the mean-squared-error over all target outputs of the model, evaluated on the training (validation) set is shown as a function of training epoch number in blue (orange). The optimizer was switched from Adam to a standard SGD optimizer after 200 epochs, producing an abrupt small decrease in the loss function on both data sets and more uniform values on the validation set.

259 climatology between 7 and 8 d. Scher and Messori (2020) compared the performance of
 260 initial-condition and retrained (i.e. SP) neural network ensembles. For the 500-hPa fore-
 261 casts using the less accurate DLWP model of Weyn et al. (2019), they found a relation-
 262 ship between the RMSE and spread in their SP ensemble roughly similar to that in Fig. 1,
 263 although in their case the spread matched the RMSE at the end of their 5-day forecast
 264 and the RMSE 500-hPa was roughly twice as large as that for our current model at the
 265 same 5-day forecast lead time (compare Fig. 5a with their Fig. 4a). In contrast to our
 266 IC ensembles, theirs was generated using singular vectors and produced only slightly less
 267 spread than their SP ensemble. Finally, as in our results, the RMSE of their IC ensem-
 268 ble mean was higher than the RMSE for their SP ensemble mean.

269 Scher and Messori (2020) did not report results for a grand ensemble consisting of
 270 both IC and SP perturbations, but given the superior ensemble spread they obtained us-
 271 ing singular vectors, such a grand ensemble might have performed substantially better
 272 than either of the individual IC or SP ensembles. In our case, a 320-member grand en-
 273 semble constructed by applying the suite of 32 DLWP models with slightly different weights
 274 to each of the 10 IC perturbations performs only very slightly better than the SP en-
 275 semble alone at 14-d forecast lead times: the RMSE and spread curves (red) for the grand
 276 ensemble almost perfectly overlap those for the SP ensemble (green) in Fig. 1. Never-
 277 theless, after bias correction (see section 3.4) the 320-member grand ensemble does per-
 278 form better than the SP ensemble at longer S2S forecast lead times.

279 3.3 The control member

280 When considering the effectiveness of ensemble forecasts, it is useful to compare
 281 the ensemble mean to a single control member. For example, in comparison to the other
 282 ensemble members, the ECMWF control forecast is run at higher horizontal (9 km) and
 283 vertical (137 levels) resolution, and without perturbations to the initial conditions. This
 284 control forecast might nominally be expected to perform better than a typical ensem-

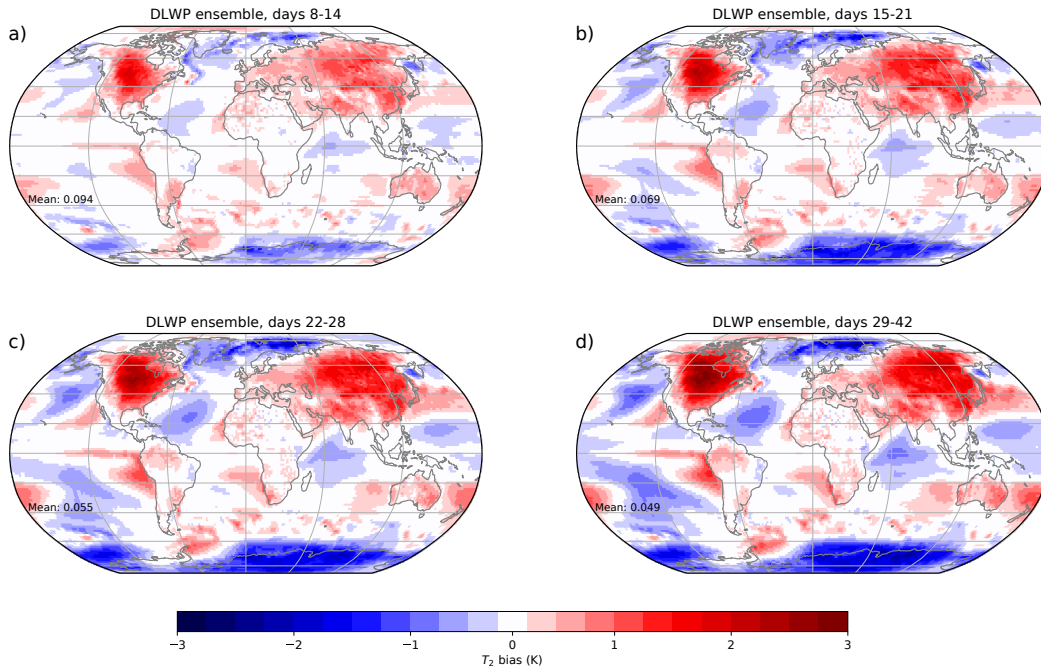


Figure 3. Bias in 2-m temperature (ensemble-mean – observation) averaged over 25 years of re-forecasts from all members of the DLWP SP ensemble: one-week averages for forecast lead times of a) 2 weeks, b) 3 weeks, c) 4 weeks, and d) a 2-week average for the week 5–6 forecast.

285 ble member that must be run at lower resolution because of computational constraints.
 286 Our control forecast is trained to better minimize the loss function using a Adam op-
 287 timizer and learning rates that decrease as the weights approach their optimum values.
 288 In particular, the learning rate starts at 10^{-3} , but once the validation-set loss does not
 289 decrease for 20 epochs, the learning rate of the optimizer is reduced by a factor of 5. This
 290 continues (up to a minimum learning rate of 10^{-6}) until a criterion of no reduction in
 291 validation loss after 50 epochs is met. The result is a model with weights that better min-
 292 imize the loss function and produces good forecasts, although in contrast to the ECMWF
 293 high-resolution control, the model used for our control forecast does not have significant
 294 advantages relative to the other ensemble members. The control forecast is initialized
 295 with the control ERA5 reanalysis data.

296 3.4 Correcting model bias

297 Unlike global climate models, NWP models are designed to make accurate predic-
 298 tions over relatively short forecast lead times without worrying about certain physical
 299 constraints, such as global radiative balance, that would be necessary for long-term cli-
 300 mate simulations. As a consequence, NWP models are typically subject to systematic
 301 drift in long-term (including sub-seasonal) forecasts. For example, previous versions of
 302 the ECMWF S2S ensemble have been shown to develop pronounced spatially-dependent
 303 patterns of mean model drift on time scales of 1–4 weeks (Vitart, 2004; Weigel et al., 2008).
 304 To compensate for this model bias, all of the major weather prediction centers produce
 305 reforecasts, or hindcasts, using their S2S ensemble prediction systems (Vitart et al., 2017),
 306 and use these reforecasts to calibrate the operational forecast products. As an example,
 307 Vitart (2004) computed the bias for a given calendar date by performing hindcasts us-
 308 ing the full ensemble initialized on the same calendar date in each of 12 previous years,
 309 and removed this bias from the forecasts in a post-processing step.

Using a strategy similar to that in Vitart (2004), we bias corrected each field by first computing ensemble reforecasts twice weekly for each DLWP SP ensemble member (and the control) on the same set of calendar dates spanning the years 1991–2015, which includes the training set and most of the validation set, but does not bleed into the 2017–2018 test set. Then, for all reforecast dates, each member’s spatially varying bias is calculated as the average of its bias on that date over the 25 year period. The bias for a specific forecast date in the test set is taken as the average reforecast bias over all available calendar dates spanning the 28-day interval centered on that forecast date, and this bias is subtracted from the forecast produced by each of the corresponding ensemble members.

Figure 3 shows spatial patterns of the annual-average model bias in 2-m temperature for the 32-member DLWP SP ensemble at forecast lead times up to 6 weeks. Warm biases are present over the northern hemisphere land masses, along with a cold bias over Antarctica. There are also warm biases in subtropical regions commonly dominated by marine stratocumulus clouds off the Pacific coasts of North and South America. These biases gradually amplify as the forecast lead time increases, although the globally averaged spatial-mean bias (noted in each panel) decreases at longer lead times. The tendency of increasing local biases to better cancel in the global mean at longer lead times is interesting and perhaps surprising because the model is only trained to minimize T_2 errors over the first 24 hours of the forecast—no global energy-balance constraints are imposed.

Bias correction has a positive impact on the control forecast and on the IC, SP, and the grand ensembles. Although the RSME and spread of the SP and grand ensembles are almost identical over the first 14 days, at longer lead times, and particularly after bias-correction, the grand ensemble is clearly superior to the SP ensemble (not shown). The performance of the grand ensemble will, therefore, be our focus throughout the remainder of this paper.

In addition to the persistence and climatology benchmarks, which serve as a baseline that must be exceeded by any skillful forecast, we will also compare our results against the state-of-the-art ECMWF 50 member S2S ensemble and a higher resolution ECMWF control simulation (Vitart et al., 2017). Errors are computed with respect to ERA5 data that is downloaded at 1 degree resolution, transformed onto our cube-sphere grid, and then transformed back to a 1.5×1.5 latitude-longitude grid. Our DLWP forecasts are transformed to the same 1.5×1.5 degree grid for the computation of all forecast metrics. The archived ECMWF S2S forecasts, available on a 1.5×1.5 degree grid, are first transformed to the cube sphere and then back to the 1.5×1.5 degree analysis grid because this procedure removed discrepancies in model terrain thereby improving the ECMWF error metrics for T_2 . Bias correction was also performed on the ECMWF S2S control and ensemble forecasts on the 1.5×1.5 degree grid, with the methodology following that of the operational ECMWF forecasts. This correction is very similar to the bias correction applied to our DLWP model, but with a few differences: the last 20 years of re-forecasts are used instead of a fixed period of 25 years; ten ensemble members with perturbed IC and physics are run for each re-forecast; and only the forecasts for dates within one week, instead of 28 days, of the target operational forecast issue date are used.

3.5 Summary

The following summarizes the construction of the DLWP grand ensemble.

1. Eight distinct training cycles of the DLWP CNN were produced with different random seeds as a first step in generating 32 stochastically perturbed (SP) models.
2. Four checkpoints during each of the eight training cycles were selected based on T_{850} ACC skill as individual SP ensemble models.

Table 2. Comparison of key attributes of our DLWP ensemble and those of the state-of-the-art ECMWF ensemble for extended-range forecasting.

	DLWP	ECMWF
Atmospheric fields	6 2-D variables	9 prognostic 3-D variables; 91 vertical levels
Horizontal resolution	150 km	18 km (36 km after day 15)
Atmospheric physics	3 prescribed inputs	Many physical parameterizations
Coupled models	None	Ocean, wave, and sea ice models
Initial condition perturbations	10 (ERA5 uncertainty)	50 (SVD/4DVAR)
Model perturbations	“Stochastic” CNN weights	Stochastic physics
Ensemble members	320 (+control)	50 (+control)

- 360 3. The model associated with each checkpoint was run on the validation data set to
361 produce 416 four-week forecasts, which were then manually inspected for forecast
362 quality. Any model that displayed irregularities was further trained with an SGD
363 optimizer. The collection of models given by these checkpoints formed the 32-member
364 SP ensemble of models. (The SGD optimizer was used in 3 of the 32 SP ensemble
365 members.)
- 366 4. Each of the 32 SP models was run with each of the 10 initial conditions (ICs) given
367 by the perturbed reanalyses in the ERA5 product to yield the 320-member grand
368 ensemble.
- 369 5. A single control DLWP model was trained slightly differently, by periodically re-
370 ducing the Adam optimizer learning rate.
- 371 6. The mean model bias for re-forecasts in the period 1991–2015 was computed for
372 the control and each SP model. That bias was removed from all the 2017-2018 test-
373 set forecasts.

374 Finally, a tabular comparison between our DLWP ensemble and the current state-
375 of-the-art ECMWF ensemble is provided in Table 2. In most regards, the ECMWF en-
376 semble is superior, with higher resolution, coupled ocean and wave models, complete physics,
377 more atmospheric variables, and better initial condition perturbations. However, our DLWP
378 ensemble consists of far more ensemble members, with 320 plus control, compared to only
379 50 plus control for the ECMWF ensemble.

380 4 Skill of the DLWP at short lead times

381 Before discussing the performance of the DLWP ensemble on S2S time scales we
382 briefly assess the qualitative skill of the model in a short deterministic forecast. We then
383 assess the quantitative skill of the DLWP control and grand ensemble in two-week fore-
384 casts relative to the state-of-the-art 50-member ECMWF S2S ensemble and the stan-
385 dard benchmarks of climatology and persistence.

386 Figure 4 compares a 4.5-day global forecast of Z_{1000} and Z_{500} with the verifying
387 analysis for 12:00 UTC, 11 September 2017, when hurricane Irma was located in the south-
388 eastern US. Irma is farther north and weaker in the DLWP forecast, but still reasonably
389 well represented for a 4.5-day forecast of such a small-scale disturbance. Other features,
390 such as the 500-hPa cutoff low west of California and the pair of short waves in the Gulf
391 of Alaska and west of Hudson Bay are also reasonably represented. On the other hand,
392 the 500-hPa cutoff low over Nova Scotia is much weaker and farther west than in the
393 verification, and the DLWP forecast does not develop the associated surface cyclone. The
394 closed surface low in the DLWP forecast over the Dominican Republic is the model’s fore-
395 cast for hurricane Jose, which is stronger and farther south than in the verification. While

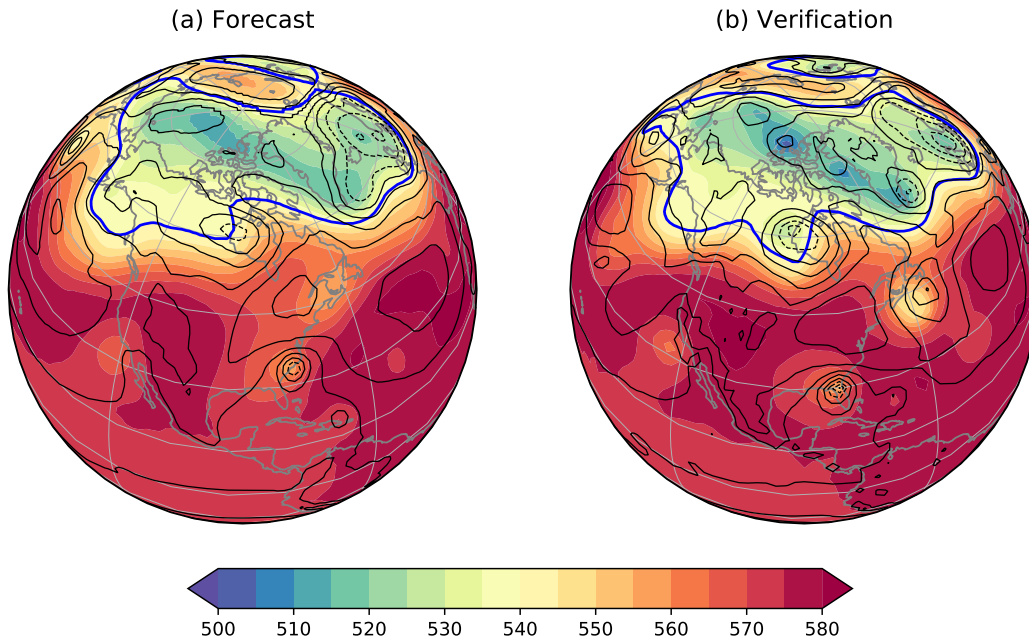


Figure 4. Fields of Z_{500} (color contours) and Z_{1000} (black contours at 100 m intervals with negative values dashed) for (a) a 4.5-day forecast and (b) the verification on 12:00 UTC, 11 September 2017. The blue curve is the 540-dm contour for Z_{500} .

396 neither perfect, nor the equal of a state-of-the-art NWP operational forecast, on the bal-
 397 ance the DLWP forecast is arguably still impressive given that it is computed at 1.4° res-
 398 olution using just 6 prognostic variables, each defined on a single spherical shell.

399 Turning to the quantitative verification of the first two weeks of forecast lead time,
 400 our cases are chosen to match the available forecast initialization times from the oper-
 401 ational S2S forecast runs at ECMWF. The DLWP model is therefore tested on 208 fore-
 402 casts initialized twice weekly starting at 00 UTC 2 January 2017, followed by the 5th,
 403 9th and 12th of January, and so on, through the end of 2018.

404 RMSE scores for Z_{500} are compared in Fig. 5a. The DLWP grand ensemble remains
 405 superior to climatology through 14 days, though unsurprisingly, its error exceeds that
 406 of the ECMWF S2S ensemble. Both the DLWP and ECMWF control forecasts perform
 407 worse than their respective ensembles, and the control-to-ensemble improvement is qual-
 408 itatively similar for both systems. At lead times beyond 9 days, the DLWP ensemble per-
 409 forms better than the ECMWF control. Similarly qualitative behaviors are apparent for
 410 the Z_{500} anomaly correlation coefficient (ACC) scores shown in Fig. 5b, although the ACC
 411 score for the ECMWF remains superior to that of the DLWP ensemble until almost day
 412 13. The persistence forecast is grossly inferior.

413 Turning now to the daily-averaged surface temperature field, which has a far more
 414 complex structure than Z_{500} , Figs. 5c,d show the performance of the DLWP models rel-
 415 ative to the ECMWF system remains similar to that for Z_{500} . (Only the daily-averaged
 416 T_2 field was available on the ECMWF archive. As shown in WDC20, the DLWP model
 417 does capture diurnal temperature variations.) The ECMWF S2S ensemble gives the best
 418 results, with its RMSE, together with that of the DLWP grand ensemble, remaining be-
 419 low the climatological benchmark through 14 days. Note that the ECMWF product uses
 420 slightly different initial conditions, which explains the substantial error in the ECMWF

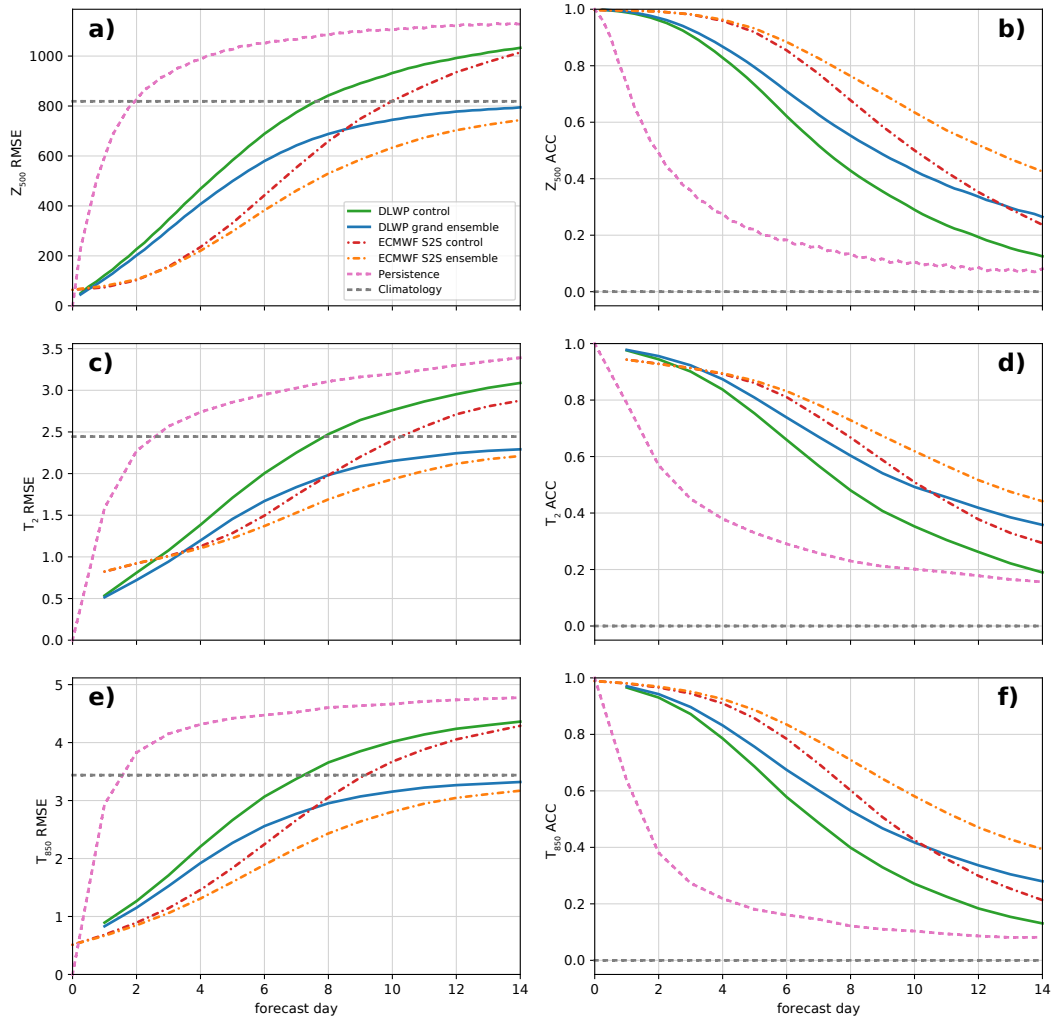


Figure 5. Forecast error as a function of time for the DLWP control member (green) and grand ensemble mean (blue), the ECMWF S2S control (dot-dashed red) and ensemble mean (dot-dashed orange), along with persistence (pink) and climatology (gray) benchmarks for twice-weekly forecasts during 2017–2018. Panels are Z_{500} : (a) RMSE (m) and (b) ACC; daily-averaged T_2 : (c) RMSE (K) and (d) ACC; T_{850} at 00 UTC: (e) RMSE (K) and (f) ACC. The error is area-weighted in latitude and globally-averaged.

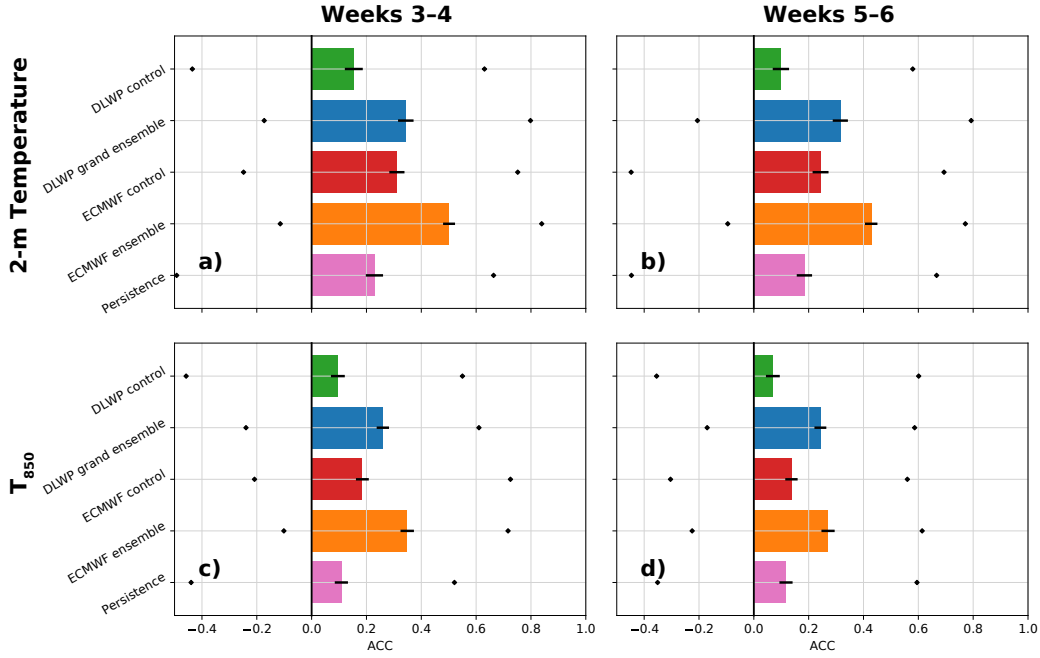


Figure 6. Anomaly correlation coefficient of 2-week-averaged forecasts from the DLWP control (green) and grand ensemble mean (blue), the ECMWF S2S control (red) and ensemble mean (orange), and persistence (pink) for forecasts made twice weekly in 2017–2018. Panels show T_2 for (a) weeks 3–4, (b) weeks 5–6, and T_{850} for (c) weeks 3–4, (d) weeks 5–6. Scores are area-weighted in latitude and globally-averaged. Black lines on each bar represent the 95% confidence interval computed using bootstrapping with 10,000 iterations. The black dots show the lowest and highest scores among the 208 forecasts.

421 RMSE at early lead times. The ACC of the DLWP ensemble again becomes superior to
 422 the ECMWF control at long lead times (after 11 days). The ability of the model to cor-
 423 rectly forecast surface temperatures using the same set of 3×3 filters over both land and
 424 ocean highlights the capability of the deep learning approach to capture processes that
 425 require complex physical parameterizations in conventional NWP models with no more
 426 information than the land-sea mask and the terrain elevation.

427 Error metrics for a third field, T_{850} , are plotted in Fig. 5e,f. This is a more diffi-
 428 cult field to forecast in the sense that the RMSE for persistence drops below the clima-
 429 tological skill threshold at shorter lead times than for Z_{500} or T_2 , and the ACC score for
 430 persistence drops below 0.4 in just two days. Nevertheless, the RMSE for the DLWP and
 431 ECMWF ensembles again remains below climatology for 14 days, with the ECMWF en-
 432 semble performing the best. The errors in the DLWP ensemble also drop below those
 433 in the ECMWF control at earlier lead times than for the other fields: 7 days for RMSE
 434 and 10 days for ACC.

435 5 Extending the forecasts to the S2S range

436 5.1 Ensemble-mean anomaly correlations

437 Globally and temporally averaged ACC scores for T_2 and T_{850} at forecast lead times
 438 of 3–4 and 5–6 weeks are compared in Fig. 6 for the DLWP and ECMWF models, along

with the persistence benchmark, for the 2017-2018 test set. Persistence forecasts are computed by averaging the observed anomalies from the 14 days prior to the forecast initialization date. At both lead times, scores are higher for T_2 than for T_{850} , reflecting greater memory in the system for near-surface temperatures than those aloft. One source of this memory are sea surface temperatures, which are closely tied to T_2 over the oceans. Unlike the ECMWF S2S model, our DLWP model does not currently include coupling with the ocean, and as a consequence, our T_2 forecast over the ocean is essentially a proxy forecast for SST. This may be one reason why the DLWP control is the only model in Fig. 6a,b that performs worse than persistence. Nevertheless for T_2 forecasts at both lead times, the DLWP ensemble is superior to both persistence and the ECMWF control. Unsurprisingly, the ECMWF ensemble gives the best results at both lead times, with an averaged ACC of roughly 0.5 for T_2 at 3–4 weeks. Turning to T_{850} , the performance of the DLWP ensemble relative to the other forecasts is better than those for T_2 . The DLWP ensemble is again superior to the ECMWF control at both lead times, and more impressively, at weeks 5–6 it is in a statistical tie with the full ECMWF S2S ensemble in the sense that the 95% confidence intervals for the forecasts overlap (black bars in Fig. 6d).

ACC scores for the best and worst individual forecasts for each period are shown by the black dots in Fig. 6. The ECMWF ensemble has the “best” worst forecasts, or the least susceptibility to bust forecasts, except for 5–6-week T_{850} , for which its ACC of -0.22 is worse than the -0.18 value for DLWP ensemble. At weeks 5–6, the best individual forecasts for both the DLWP and ECMWF ensembles have ACC scores of about 0.8 for T_2 and about 0.6 for T_{850} . The globally averaged ACC for the 3–4-week T_2 forecasts exceeds 0.5 roughly 25% of the time for the DLWP grand ensemble and 50% of the time for the ECMWF ensemble.

An example of a good (though not the best) 3–4-week T_2 anomaly forecast for both ensembles is shown in Fig. 7. These forecasts were initialized on 27 September 2018. The intensity and spatial variability in the DLWP control forecast are grossly similar, although modestly weaker and smoother, than those in the ECMWF control, demonstrating that the DLWP forecast is not simply approaching a smooth climatology at long forecast lead times. Similarly, the forecast from the 320-member DLWP grand ensemble exhibits much of the intensity and spatial variability in the 50-member ECMWF ensemble forecast. (Although the horizontal resolution of the ECMWF S2S ensemble members is 31 km beyond lead times of 15 days, the data are archived at coarser resolution and all forecasts are displayed on a $1.5^\circ \times 1.5^\circ$ latitude-longitude grid.)

Anomalies that both verify (Fig. 7f) and are common to the DLWP (Fig. 7a) and ECMWF S2S (Fig. 7b) ensembles include cold in Greenland and warmth in eastern Australia, eastern Siberia and over the adjacent Arctic Ocean. One place where the ECMWF S2S ensemble clearly outperforms the DLWP ensemble is over North America, where it better captures the observed large and intense cold anomaly. Another important superiority of the ECMWF ensemble lies in its forecast of a developing El Niño over the equatorial Pacific, although the absence of the El Niño in the DLWP ensemble forecast is not particularly surprising because it does not include any oceanic data.

5.2 Ensemble probabilistic scores

Having just examined the ACC scores of the ensemble mean, we now investigate the performance of ensemble-produced probabilistic forecasts, specifically the continuous ranked probability score (CRPS) and the ranked probability skill score (RPSS).

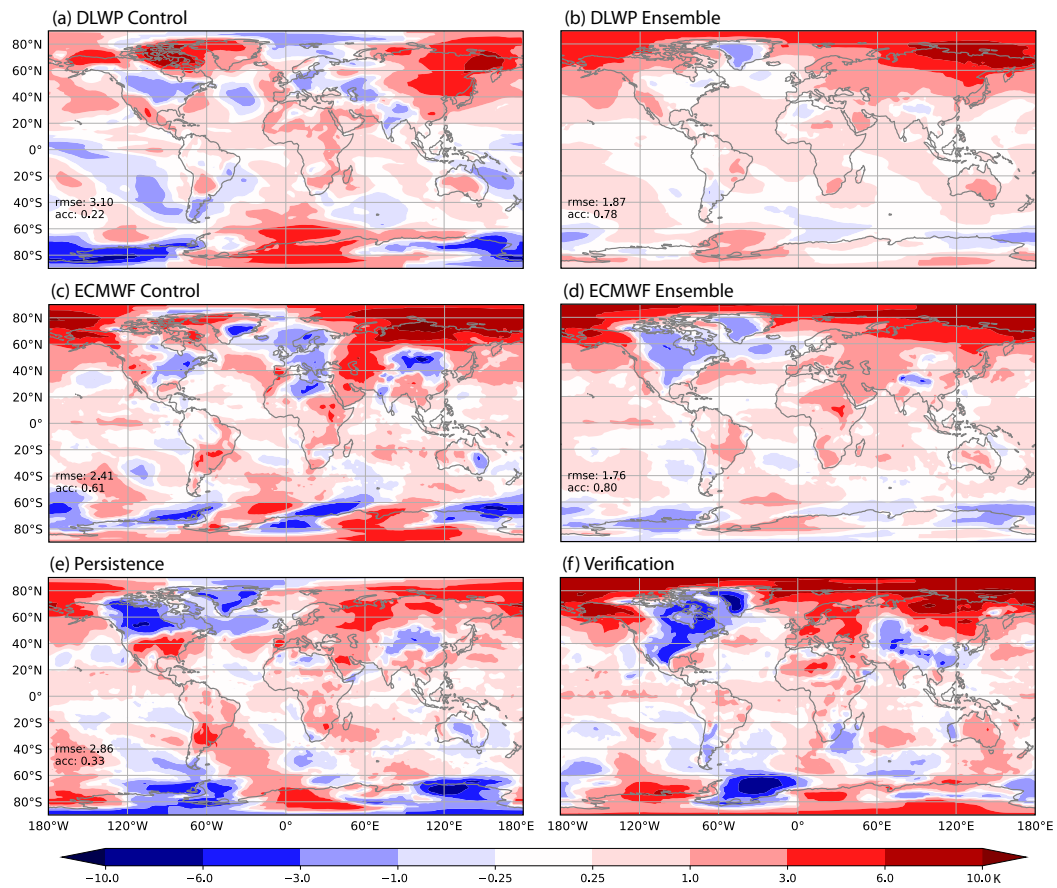


Figure 7. Predicted 2-week average anomalies in T_2 relative to climatology for the period 3–4 weeks after 27 September 2018. Forecasts are from DLWP (a) control and (b) grand ensemble, ECMWF S2S (c) control and (d) ensemble, and (e) persistence; (f) is the verification. The ‘rmse’ and ‘acc’ numbers are global averages; the rmse is the root-mean-squared error of the *anomalies*.

485

5.2.1 Continuous ranked probability score

Denoting the ensemble probability distribution function of a forecast for some variable x as $\rho(x)$, the cumulative distribution function (CDF) associated with ρ is

$$P(x) = \int_{-\infty}^x \rho(y) dy. \quad (1)$$

If the verifying value occurs at x_a , a CDF for the observation may be defined as

$$P_a(x) = H(x - x_a), \quad (2)$$

where

$$H(s) = \begin{cases} 0 & s < 0 \\ 1 & s \geq 0 \end{cases} \quad (3)$$

is the Heaviside function. The CRPS may then be defined as (Hersbach, 2000):

$$\text{CRPS} = \text{CRPS}(P, x_a) = \int_{-\infty}^{\infty} [P(x) - P_a(x)]^2 dx. \quad (4)$$

486

487

488

489

490

491

492

493

494

The CRPS score penalizes both overly narrow (confident) forecast distributions that verify incorrectly and overly broad (uncertain) forecast distributions, regardless of the accuracy of the ensemble mean. The CRPS has several desirable properties. First, it is a proper statistical score (Gneiting & Raftery, 2007), meaning that the CRPS is optimized for a forecast which predicts the correct probability distribution of a predicted variable. Second, in contrast to categorical scores, such as the RPSS (see Section 5.2.2), it accounts for information across all possible values of x . Finally, the CRPS reduces to the mean absolute error for a single deterministic forecast, allowing the performance of ensemble and deterministic forecasts to be easily compared.

495

496

497

498

499

500

501

502

503

504

505

506

507

Figure 8 compares CRPS in T_{850} for forecasts from the DLWP and ECMWF S2S ensembles and control forecasts, along with persistence and climatology benchmarks, averaged over one week for lead times of 2, 3 and 4 weeks, along with a two-week average for a lead time of 5–6 weeks. As with our earlier results for the T_{850} RMSE and ACC of the ensemble mean (Fig. 5), the ECMWF ensemble clearly gives better week-2 CRPS scores than the DLWP ensemble. At week 3, when deterministic forecast skill from initial conditions has largely eroded, the ECMWF ensemble continues to give a slightly better global mean result. But by week 4 and weeks 5–6, the DLWP ensemble has caught up and is essentially tied with ECMWF (Fig. 8a). At lead times of three weeks or longer, the next best global-mean forecasts are given by climatology, which out-performs the ECMWF and DLWP control forecasts, which are in turn better than persistence. Note that all CRPS scores except persistence improve significantly from week 4 to weeks 5–6 due to the longer two-week averaging window.

508

509

510

511

512

513

514

515

516

517

518

519

Focusing on the tropics, from 20°S to 20°N, the CRPS for all models are substantially improved, with numerical values roughly 0.4 times the corresponding global results (Fig. 8b). The ECMWF and DLWP ensembles still perform the best, and the relative performance of the various forecast systems is similar to the globally-averaged results, although the ECMWF ensemble scores are slightly improved relative to the DLWP ensemble. CRPS scores are worse in the northern hemisphere extra-tropics, 30°N – 90°N (Fig. 8c,d), and there is a pronounced seasonality in performance. The scores are worse in boreal winter, and the performance of the DLWP ensemble relative to the ECMWF ensemble is also worse. On the other hand, in boreal summer, the CRPS values improve and the DLWP ensemble ties ECMWF in weeks 3, 4 and 5–6. This seasonal difference in extra-tropical performance suggests that the DLWP model performs worse relative to ECMWF when synoptic-scale dynamics exert more influence on the weather.

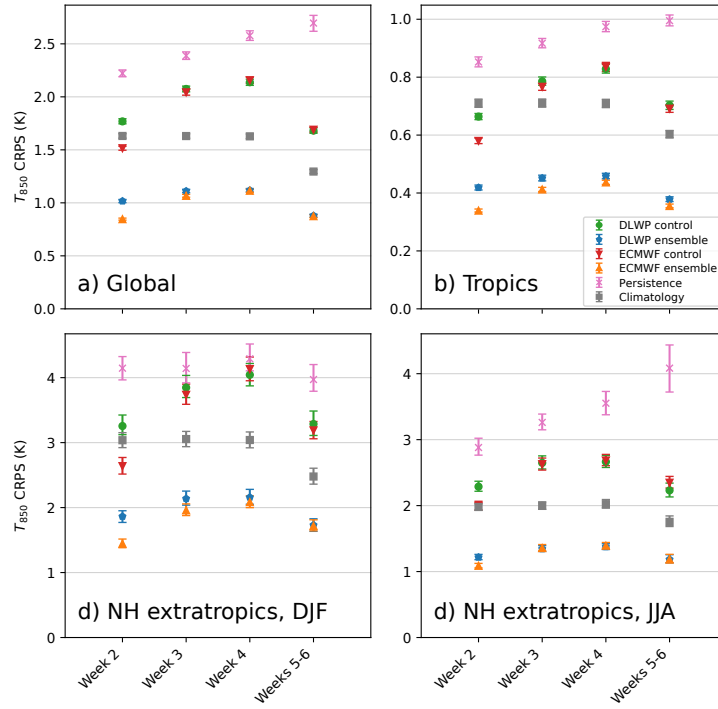


Figure 8. Continuous ranked probability score (CRPS; lower is better) in T_{850} from the DLWP control (green circles), DLWP grand ensemble (blue pentagons), ECMWF S2S control (red downward pointing triangles), ECMWF ensemble (orange upward pointing triangles), persistence (pink crosses), and climatology (gray squares), as a function of averaged forecast-lead time. Panels show: a) Global average, annual mean; b) average over the tropics ($20^{\circ}\text{S} - 20^{\circ}\text{N}$), annual mean; c) average over the northern hemisphere extra-tropics ($30^{\circ}\text{N} - 90^{\circ}\text{N}$), mean of forecasts initialized in DJF; d) average over the NH extra-tropics, JJA. Error bars correspond to the 95% confidence interval determined by bootstrapping with 10,000 samples.

520

5.2.2 Ranked probability skill score

521

522

523

524

525

526

527

528

The other metric we use to evaluate the ensemble forecasts is the ranked probability skill score (RPSS). To compute the RPSS, K categorical forecasts are first defined. Then let y_i be the probabilistic forecast of the event occurring in category i ; let c_i be the climatological probability of the event falling in category i , and bin the verification such that $o_i = 1$ if the event was observed to be in category i and $o_i = 0$ otherwise. The k th components of the cumulative forecast, climatological, and observational distributions Y_k , C_k , and O_k are evaluated for each of the K categories as $Y_k = \sum_{i=1}^k y_i$, $C_k = \sum_{i=1}^k c_i$, and $O_k = \sum_{i=1}^k o_i$.

Ranked probability scores for the forecast (RPS) and climatology (RPS_C) are computed as

$$\text{RPS} = \sum_{k=1}^K (Y_k - O_k)^2 \quad (5)$$

$$\text{RPS}_C = \sum_{k=1}^K (C_k - O_k)^2, \quad (6)$$

and finally, using angled brackets to denote the average over all forecast-observation pairs, the RPSS is defined as

$$\text{RPSS} = 1 - \frac{\langle \text{RPS} \rangle}{\langle \text{RPS}_C \rangle}. \quad (7)$$

The RPS is zero for a perfect forecast and increases positively otherwise, therefore the RPSS for a perfect forecast is one and decreases otherwise. Normalizing $\langle \text{RPS} \rangle$ by $\langle \text{RPS}_C \rangle$ in (7) sets the threshold value below which there is no skill relative to climatology to zero. Like the CRPS, the RPSS is a proper score, but it does depend on the definition of categories. The RPSS is sensitive to the size of the ensemble, having a negative bias for small ensemble sizes (Weigel et al., 2007). Although both the grand ensemble size of 320 and the ensemble size of 50 for ECMWF are large enough to mitigate such bias, in lieu of (7) we will use the de-biased formulation of the RPSS (Weigel et al., 2007), which for ensemble size M is

$$\text{RPSS} = 1 - \frac{\langle \text{RPS} \rangle}{\langle \text{RPS}_C \rangle + D_0/M} \quad (8)$$

$$D_0 = \frac{K^2 - 1}{6K}. \quad (9)$$

529

530

531

532

533

534

535

536

537

538

539

540

541

We compute the RPSS for T_2 and T_{850} , binning into three climatologically equally-likely terciles of below-, near-, and above-normal relative to the baseline period of 1981–2010. Tercile bounds for T_2 were determined from daily-averaged values (using the times 0, 6, 12, and 18 UTC) for each date in the 30-year record. These daily tercile bounds are then averaged over each one- or two-week verification period. For T_{850} , only the instantaneous 0 UTC values were available from the ECMWF S2S database, therefore a separate climatology is computed from only 0 UTC values to evaluate the ECMWF model (the DLWP forecasts are daily-averaged and evaluated using terciles computed from the daily averages). Because each of the forecast categories are, by design, equally likely, the climatological forecast is simply a 33% likelihood of occurrence in each of the categories. Note that because (5) and (6) use cumulative distributions, events verifying in the near-normal category have lower expected random-chance forecast error than events verifying in either the below- or above-normal categories.

542

543

544

545

Spatially- and temporally-averaged RPSS scores in T_{850} from the DLWP and ECMWF S2S ensembles are shown in Fig. 9. The globally-averaged RPSS (Fig. 9a) for the DLWP ensemble is well above the zero threshold for random chance at all lead times. Comparing Figs. 8 and 9, and recalling that, in contrast to the RPSS, lower CRPS scores are

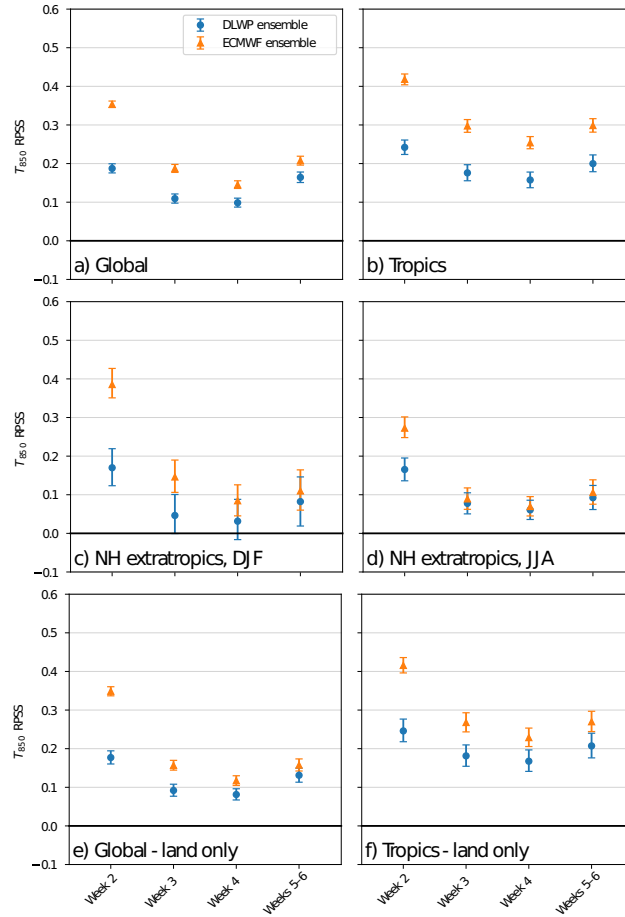


Figure 9. One- or two-week averaged ranked probability skill score (RPSS; higher is better) for T_{850} at indicated forecast lead times. DLWP grand ensemble (blue circles) and the ECMWF S2S ensemble (orange triangles) averaged over the (a) globe, annual mean; (b) tropics ($20^{\circ}\text{S} - 20^{\circ}\text{N}$), annual mean; (c) NH extra-tropics ($30^{\circ}\text{N} - 90^{\circ}\text{N}$), mean of forecasts initialized in DJF; (d) NH extra-tropics, mean over JJA; (e) and (f), as in (a) and (b) except spatially averaged only over land. Error bars correspond to the 95% confidence interval determined by bootstrapping with 10,000 samples.

Table 3. RPSS scores for T_2 for three S2S lead times, debiased for ensemble size, averaged globally for twice weekly forecasts in years 2017-2018 from the ECMWF and DLWP ensembles. Column ECMWF 2011 gives the same except for reforecasts covering the years 1995–2001 using the ECMWF ensemble as formulated in 2011.

Days	ECMWF	DLWP	ECMWF 2011
12–18	0.247 ± 0.017	0.121 ± 0.016	0.135 ± 0.021
19–25	0.167 ± 0.016	0.083 ± 0.016	0.054 ± 0.026
26–32	0.145 ± 0.015	0.076 ± 0.015	0.030 ± 0.009

546 better, both metrics show similar variations in ensemble skill with forecast lead time in
 547 all regions and over all time windows. The superiority of the ECMWF ensemble is, nev-
 548 ertheless, greater in the RPSS metric, with a statistically-significant lead over our DLWP
 549 ensemble at all forecast lead times and locations, except during JJA in the northern hemi-
 550 sphere extratropics (Fig. 9d). The performance difference between the two ensembles is
 551 significantly reduced if we consider only locations over land as shown in Fig. 9e,f, where
 552 the skill of the ECMWF ensemble drops significantly after Week 2 while the RPSS for
 553 the DLWP ensemble, which has no information about SST, remains similar to that over
 554 both land and water shown in Fig. 9a,b.

555 A similar analysis of the ECMWF ensemble RPSS, also debiased for ensemble size,
 556 was presented in Vitart (2014) for the NH extratropics (north of 30° N) and slightly dif-
 557 ferent weekly periods of 12-18, 19-25 and 26-32 days. In Table 3, the performance of the
 558 DLWP and current ECMWF S2S ensembles are compared with data taken from Fig. 12a
 559 of Vitart (2014), which gives the average performance of a five-member ensemble of re-
 560 forecasts using the 2011 ECMWF forecast system in twice-weekly forecasts over the years
 561 1995–2001. Because sub-seasonal forecast skill can vary from year to year depending on
 562 slowly evolving large-scale circulation patterns, caution must be used when comparing
 563 their results averaged over 1995–2001 to our calculations for 2017-2018. Nevertheless,
 564 within the limitations of such comparison, it is worth noting that the DLWP grand en-
 565 semble performs better than the 2011 ECMWF forecast system at lead times of 19–25
 566 and 26–32 days.

567 The global pattern of RPSS scores, averaged over all of the forecasts in the 2017–
 568 2018 test set, is shown by the maps of RPSS scores for both ensembles at weeks 3, 4, and
 569 5–6 in Fig. 10. As expected from the plot of global average scores in Fig. 9a, the ECMWF
 570 ensemble is superior to the DLWP ensemble, with the two becoming more alike and show-
 571 ing more skill in the forecasts averaged over the longer two-week period, weeks 5–6. Par-
 572 ticularly at weeks 5–6 (Fig. 10e,f), the distribution of the low- and high-skill regions in
 573 the DLWP and ECMWF ensembles are quite similar. Both ensembles perform almost
 574 the same over land and both do very well over the Southern Ocean. The DLWP ensem-
 575 ble shows skill in the tropical oceans, but the ECMWF ensemble does much better in
 576 that region, and it largely avoids the loss of skill suffered by the DLWP ensemble over
 577 the adjacent subtropical waters. As mentioned previously, our DLWP model likely suf-
 578 fers from the absence of information about SSTs.

579 The seasonal variation in RPSS at 5-6 weeks is shown in Fig. 11. The performance
 580 of the DLWP and ECMWF ensembles is most similar in MAM, with global RPSS av-
 581 erages of 0.180 and 0.191, respectively, and analogous spatial patterns of high and low
 582 skill. As in the annual mean (Fig. 10e,f), the skill is relatively high over the tropical and
 583 southern oceans. The seasonal averages show more pronounced localized regions of high
 584 and no skill ($\text{RPSS} < 0$). One local area where both ensembles show skill, with the DLWP
 585 performing best, is in the storm track off the east coast of North America in both DJF
 586 and SON. The worst globally-averaged RPSS for both ensembles, and the worst perfor-

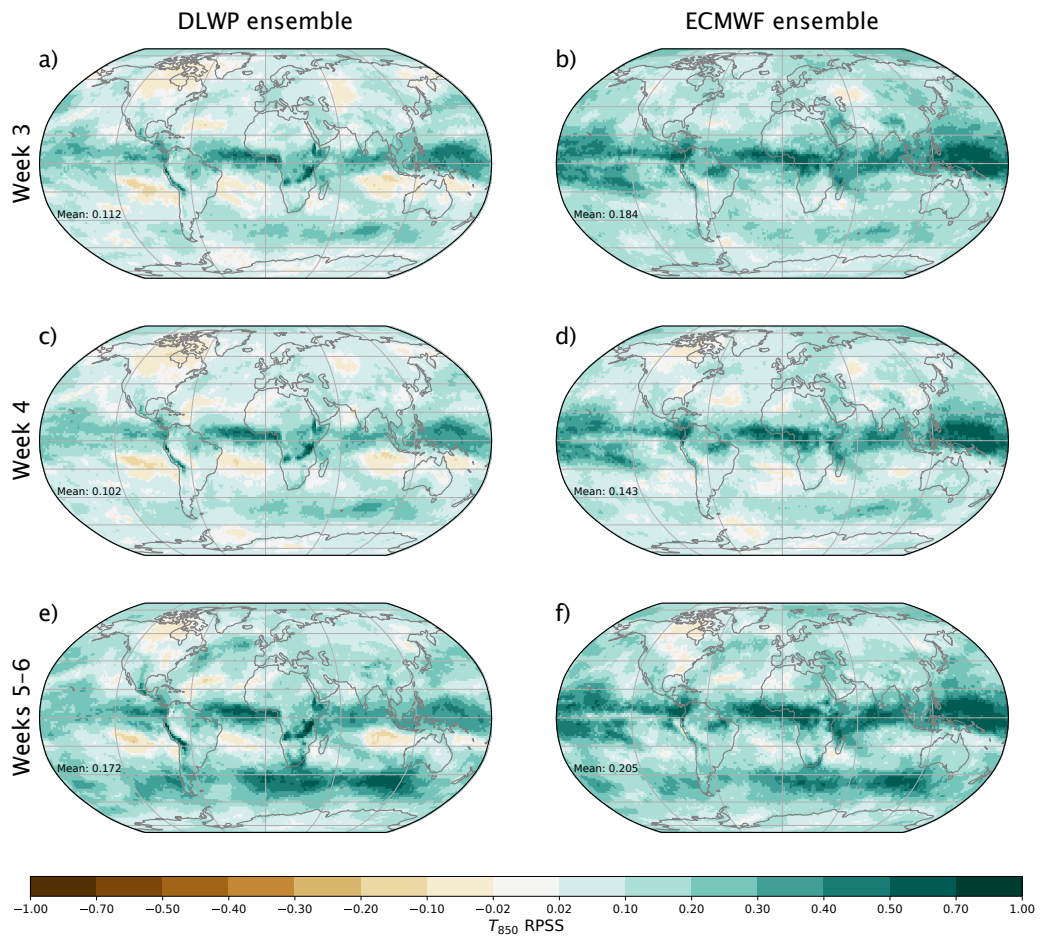


Figure 10. Annual average over the 2017–2018 testing period of T_{850} RPSS scores. Left (right) column show DLWP (ECMWF) ensembles at forecast lead times of (a), (b): 3 weeks, (c), (d) 4 weeks, and (e), (f) 5–6 weeks. The weighted global mean is noted in each panel.

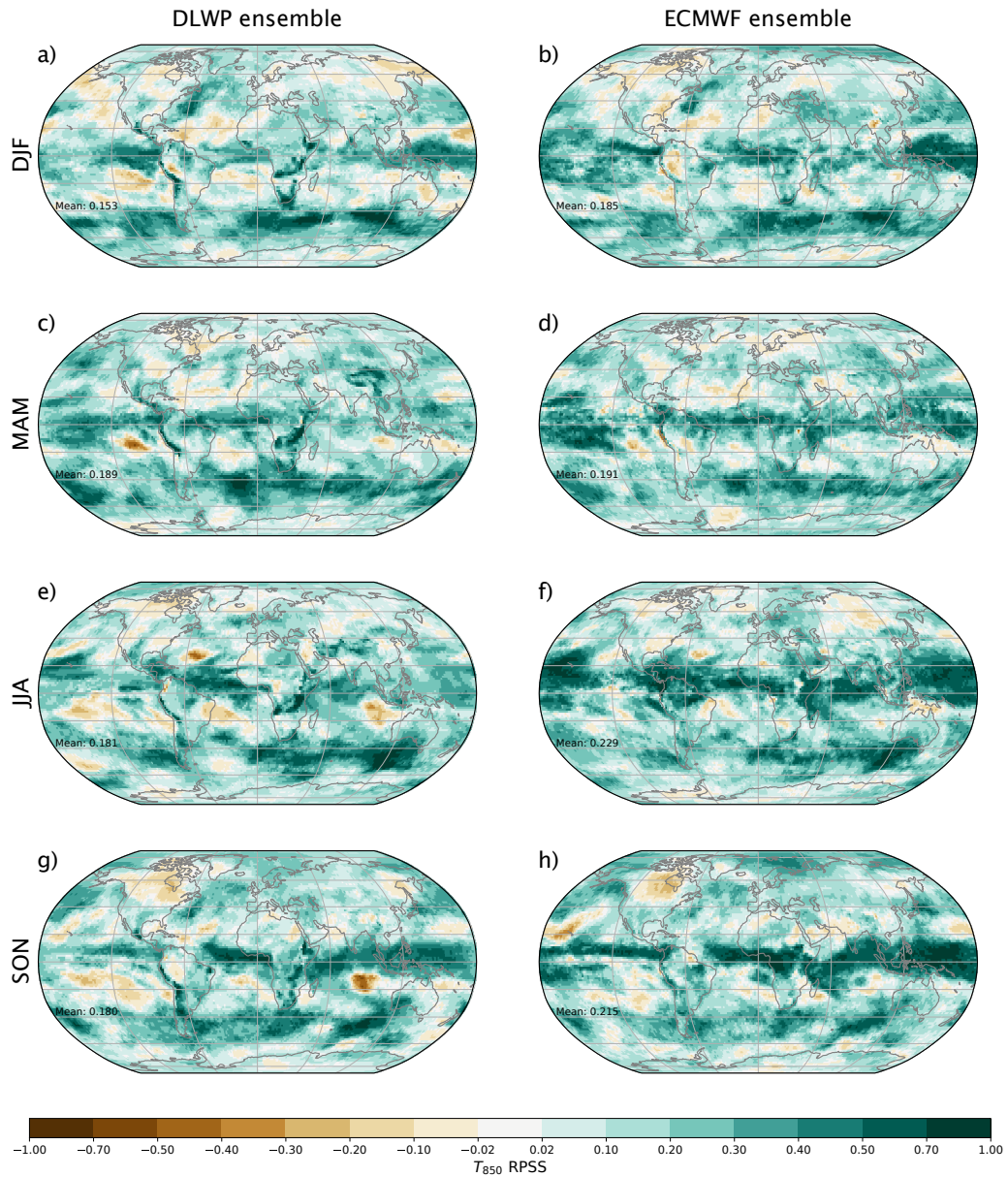


Figure 11. Maps of seasonally averaged RPSS scores in T_{850} during the testing period of 2017–2018. Left (right) column DLWP (ECMWF S2S) ensembles at 5–6 weeks forecast lead time for months (a), (b): DJF, (c), (d) MAM, (e), (f) JJA, and (g), (h) SON. The weighted global mean is noted in each panel.

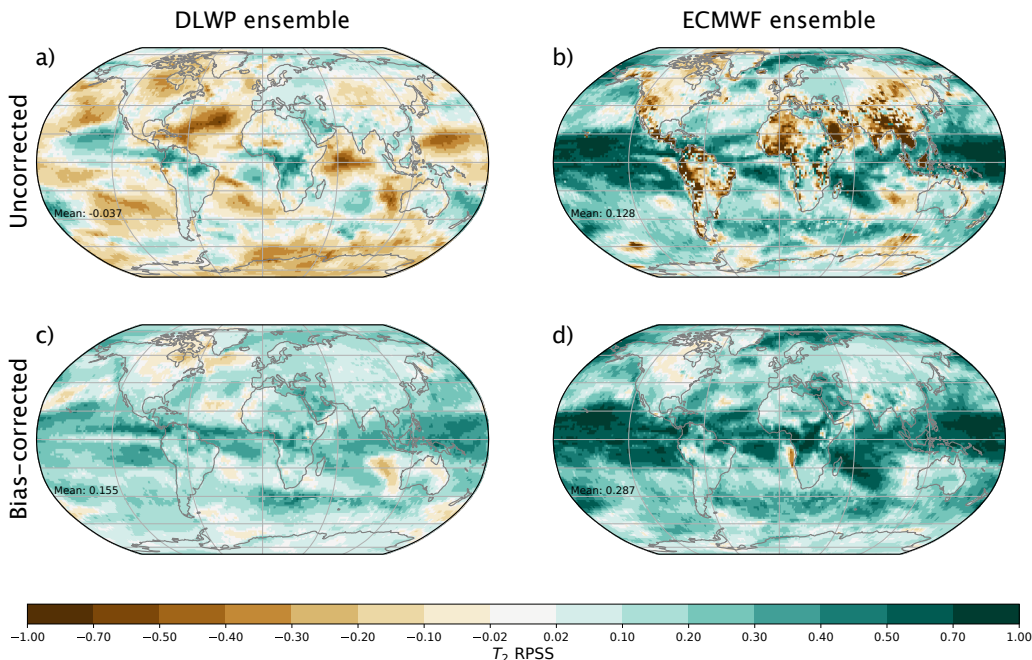


Figure 12. Annual average RPSS skill maps for T_2 at weeks 5–6. Without bias correction: (a) DLWP ensemble, (b) ECMWF ensemble; with bias correction: (c) DLWP ensemble, (d) ECMWF ensemble. The weighted global mean is noted in each panel.

587 mance of DLWP relative to ECMWF, occurs during DJF, but even in this season the
588 spatial patterns of high and low skill are similar.

589 Finally, we consider surface temperature anomalies, which, as might be expected
590 given the pronounced model drift evident in Fig. 3, are significantly improved by bias
591 correction. Maps of RPSS for both the DLWP and ECMWF ensemble forecasts for weeks
592 5–6 are shown in Fig. 12. Bias correction significantly improves the RPSS over land for
593 both ensembles, with much of that improvement in the ECMWF model coming from re-
594 gions with topography where removing the bias helps correct for differences in the way
595 the orography is represented at different grid resolutions. Bias removal also makes large
596 improvements over the oceans in the DLWP ensemble, perhaps partly compensating for
597 the lack of SST data. The regions of highest skill in the bias-corrected forecasts from both
598 ensembles are mostly over the oceans, particularly in the tropics. The global mean RPSS
599 for both ensembles, 0.155 for DLWP and 0.287 for ECMWF, are non-negative, indicat-
600 ing modest skill relative to climatology. The results for the bias-corrected ECMWF en-
601 ssemble (Fig. 3d) are generally consistent with the distribution of RPSS scores from an
602 earlier version of the ECMWF ensemble in (Weigel et al., 2008), which showed skill pre-
603 dominantly over tropical oceans after week 2, despite accounting for bias correction in
604 the forecasts. Improvements in the ECMWF model since (Weigel et al., 2008) have, nev-
605 ertheless, led to generally higher RPSS values over the oceans and much better perfor-
606 mance over the Western Pacific and Indian Oceans, as would be apparent in a compar-
607 ison of these results with their Fig. 4, although such comparison must be qualified by
608 noting the current forecasts and those in (Weigel et al., 2008) verify in different years.

609 The tendency of the 5–6 week bias-corrected T_2 ECMWF ensemble forecast to per-
610 form similarly to the DLWP forecast over land, and better over the oceans, is again ap-
611 parent in the seasonal results for SON shown in Fig. 13. Note in particular, the nega-

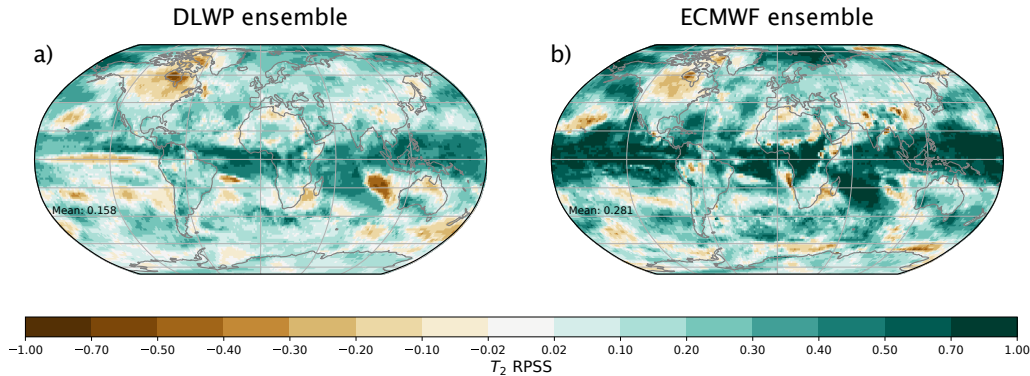


Figure 13. As in Fig. 12, but only for bias-corrected forecasts initialized in SON.

612 tive RPSS score over the equatorial eastern Pacific Ocean, which arises because the DLWP
 613 ensemble fails to correctly capture the onset of a weak El Niño event in 2018. In con-
 614 trast, the ECMWF ensemble, with coupling to an ocean model, exhibits high skill through-
 615 out the same region.

616 6 Conclusions

617 As a first step toward developing a deep-learning-based ensemble system for S2S
 618 forecasting, we refined our previous data-driven global model (Weyn et al., 2020) by im-
 619 proving the resolution at the equator to approximately 1.4° by 1.4° and by adding two
 620 more physical fields, the temperature at 850 hPa and total column water vapor. These
 621 refinements allowed the model to both spontaneously generate tropical cyclones and also
 622 produce a reasonable, though far from state-of-the-art, four-day deterministic forecast
 623 of hurricane Irma. Despite the higher resolution and the expansion from four to six spher-
 624 ical shells of prognostic variables, the model remains very computationally efficient. A
 625 one-week forecast, stepped forward with a 12-hour time step (and 6-hour resolution), can
 626 be performed in approximately 1/10th of a second on an Nvidia Tesla V100 graphics pro-
 627 cessing unit (GPU).

628 We exploited this efficiency to generate large ensemble forecasts. Only about 3 min-
 629 utes are required to produce a 320-member six-week ensemble forecast. Those 320 en-
 630 semble members were generated by running 32 different DLWP models, trained to slightly
 631 different convolutional filter coefficients, on each of 10 initial conditions. The initial con-
 632 ditions were non-optimal; rather than including information from singular vectors, they
 633 were simply drawn from the ERA5 archive. The strategy of training DLWP models with
 634 slightly different filter coefficients was, on the other hand, very effective, adding signif-
 635 icant skill to the ensemble mean and greatly increasing the ensemble spread (Figs. 1 and
 636 5). The ensemble spread introduced by the 32 similar DLWP models is functionally anal-
 637 ogous to that of conventional NWP ensemble members with stochastically perturbed phys-
 638 ical parameterization tendencies or stochastic kinetic energy backscatter. Our DLWP
 639 model requires 6–8 days of computation to train on a single Tesla V100 GPU. We were
 640 able to economize by training only eight of our 32 “physics-ensemble” members from scratch
 641 with different initial seeds and filling out the ensemble with models using filter coeffi-
 642 cients from different checkpoints saved during the eight training iterations.

643 As was also the case for the ECMWF S2S forecast, the DLWP ensemble mean fore-
 644 cast was a significant improvement over that from a single control member. In partic-
 645 ular, the average RMSE over the 2017–2018 test set of DLWP ensemble forecasts for Z_{500} ,

646 T_{850} , and 2-m temperature remained below climatology for at least 14 days, while the
 647 anomaly correlation coefficients remained above 0.6 for 7–8 days. Not surprisingly the
 648 ECMWF S2S ensemble did perform better, particularly at earlier lead times, and it also
 649 gave ACC scores exceeding the 0.6 threshold out to 10 days. At longer lead times, week
 650 3–4 or week 5–6 averages, the ACC scores of the ECMWF and DLWP ensemble means
 651 were positive and better than persistence, but still relatively low. The 2017–2018 aver-
 652 aged scores ranged from roughly 0.25 to 0.5, with the ECMWF ensemble performing bet-
 653 ter in all cases except for T_{850} at weeks 5–6, for which both ensembles were in a statisti-
 654 cal tie with an ACC of approximately 0.25.

655 We examined two probabilistic measures of ensemble skill, the CRPS and RPSS.
 656 The DLWP and ECMWF S2S ensembles produce essentially the same week-4 and weeks-
 657 5–6 CRPS scores. At shorter lead times the ECMWF ensemble is superior, performing
 658 marginally better at week 3 and distinctly better than the DLWP ensemble at week 2.
 659 Both the DLWP and ECMWF ensembles clearly out-performed climatology and persis-
 660 tence. Examining seasonal and regional contrasts showed that in the northern hemisphere
 661 extra-tropics, the DLWP ensemble performed best, and on a par with the ECMWF en-
 662 semble in the summer season; while performing worst in winter.

663 Like the CRPS, the spatially- and temporally-averaged RPSS scores showed mod-
 664 est skill relative to climatology at all lead times. The ECMWF ensemble RPSS scores
 665 exceeded those of the DWLP ensemble by larger margins than in the CRPS metric, ex-
 666 cept in summer in the northern extra-tropics when both ensembles again achieved simi-
 667 lar scores. In both the globally-averaged and tropics-only-averaged RPSS, the differ-
 668 ential by which the ECMWF RPSS score exceeds that of DLWP is smaller over land than
 669 over the full globe. Global maps comparing the ECMWF and DLWP RPSS scores show
 670 generally similar regions of higher and lower skill, except that the ECMWF ensemble per-
 671 forms better over the tropical oceans. At weeks 5–6, the spatial distribution of regions
 672 of skill and no-skill in the RPSS metric over land are surprisingly similar between the
 673 ECMWF and DLWP ensembles (Fig. 11). One reason the DLWP model performs poorer
 674 over the tropical oceans is likely due to its lack of SST data, as suggested by its failure
 675 in the eastern equatorial Pacific during the onset of a weak El Niño event in 2018.

676 Although our current data-driven DLWP model is worse than operational NWP
 677 models for the deterministic prediction of synoptic-scale weather patterns, its capabil-
 678 ity to learn physics-based phenomena, including the complex evolution of near-surface
 679 temperatures and long-term patterns in the convection-dominated tropics, is remarkable.
 680 As such, DLWP may prove a valuable tool for supplementing NWP-based S2S forecasts
 681 where they are weakest: in the tropics and in the spring and summer months.

682 There are many avenues for further development of our elementary DLWP ensem-
 683 ble system. One obvious shortcoming is that our DLWP model does not yet forecast pre-
 684 cipitation. This might be addressed by adding precipitation to the current set of six prog-
 685 nostic 2D fields that are recursively stepped forward by the model, although instead of
 686 including the precipitation at previous times in the CNN architecture, it could alterna-
 687 tively be diagnosed from the other fields after each step (Larraondo et al., 2019).

688 The DLWP model’s computational efficiency can be used for more than simply pro-
 689 ducing timely operational forecasts; it also enables researchers to make unprecedented
 690 use of large numbers of reforecasts for past weather events. We computed 25 years of re-
 691 forecasts, with 104 forecasts per year for 33 ensemble members, in a matter of hours on
 692 a single GPU. We only used these reforecasts to correct the average drift in the DLWP
 693 model, but one could also use them to calibrate ensemble probability distributions, ana-
 694 lyze model errors, or investigate of the sources of predictability captured by the model.
 695 Historically, adjoint models (e.g., Doyle et al., 2014), which are tangent linear, differen-
 696 tiable approximations to full non-linear dynamical NWP models, have been used to ex-
 697 amine how model errors depend on initial condition uncertainties (for example, whether

698 errors in moisture over the US have a strong influence on the location or intensity of a
 699 cyclone over Europe). Adjoint models are difficult to create for complex operational NWP
 700 models. Yet, because a CNN is fully differentiable, it is easy to produce the correspond-
 701 ing adjoint model, enabling studies of error growth and atmospheric predictability. Re-
 702 cent work on the interpretation of deep neural networks may provide some valuable tools
 703 for this form of analysis (Toms et al., 2020; Ebert-Uphoff & Hilburn, 2020).

704 **Acknowledgments**

705 J. A. Weyn and D. R. Durran’s contributions to this research were funded by Grant N00014-
 706 17-1-2660 from the Office of Naval Research (ONR). D. R. Durran was also supported
 707 by Grant N00014-20-1-2387 from ONR. J. A. Weyn was also supported by a National
 708 Defense Science and Engineering Graduate (NDSEG) fellowship from the Department
 709 of Defense (DoD). Computational resources were provided by Microsoft Azure via a grant
 710 from Microsoft’s AI for Earth program. Stan Posey (Nvidia) also generously donated two
 711 V100 GPUs to the University of Washington which were used for this work.

712 **Data Availability Statement**

713 The ERA5 reanalysis data are available via the Copernicus Climate Data Store (DOI:
 714 10.24381/cds.bd0915c6 and DOI: 10.24381/cds.adbb2d47). The ECMWF S2S forecasts
 715 are available at <https://apps.ecmwf.int/datasets/data/s2s>. The T42 and T63 IFS fore-
 716 casts are available from Rasp et al. (2020b).

717 **References**

- 718 Adames, Á. F., & Kim, D. (2016, March). The MJO as a dispersive, convectively
 719 coupled moisture wave: Theory and observations. *Journal of the Atmospheric*
 720 *Sciences*, *73*(3), 913–941. doi: 10.1175/JAS-D-15-0170.1
- 721 Bauer, P., Thorpe, A., & Brunet, G. (2015). The quiet revolution of numerical
 722 weather prediction. *Nature*, *525*(7567). doi: 10.1038/nature14956
- 723 Buizza, R. (2019). Introduction to the special issue on “25 years of ensemble fore-
 724 casting”. *Quarterly Journal of the Royal Meteorological Society*, *145*(S1), 1–11.
 725 doi: 10.1002/qj.3370
- 726 Doyle, J. D., Amerault, C., Reynolds, C. A., & Reinecke, P. A. (2014). Initial
 727 condition sensitivity and predictability of a severe extratropical cyclone
 728 using a moist adjoint. *Monthly Weather Review*, *142*(1), 320–342. doi:
 729 10.1175/MWR-D-13-00201.1
- 730 Dueben, P. D., & Bauer, P. (2018). Challenges and design choices for global weather
 731 and climate models based on machine learning. *Geoscientific Model Develop-*
 732 *ment*, *11*(10), 3999–4009. doi: 10.5194/gmd-11-3999-2018
- 733 Ebert-Uphoff, I., & Hilburn, K. A. (2020, may). Evaluation, Tuning and Interpret-
 734 ation of Neural Networks for Meteorological Applications. *ArXiv*. Retrieved
 735 from <http://arxiv.org/abs/2005.03126>
- 736 Fortin, V., Abaza, M., Anctil, F., & Turcotte, R. (2014, Aug). Why should ensemble
 737 spread match the rmse of the ensemble mean? *J. Hydrometeorol.*, *15*(4),
 738 1708–1713. doi: 10.1175/JHM-D-14-0008.1
- 739 Gneiting, T., & Raftery, A. E. (2007). Strictly proper scoring rules, prediction,
 740 and estimation. *Journal of the American Statistical Association*, *102*(477),
 741 359–378. doi: 10.1198/016214506000001437
- 742 Hersbach, H. (2000). Decomposition of the continuous ranked probability score for
 743 ensemble prediction systems. *Weather and Forecasting*, *15*(5), 559–570. doi: 10
 744 .1175/1520-0434(2000)015<0559:DOTCRP>2.0.CO;2
- 745 Hwang, J., Orenstein, P., Cohen, J., Pfeiffer, K., & Mackey, L. (2019, sep).
 746 Improving subseasonal forecasting in the western U.S. With machine
 747 learning. In *Proceedings of the acm sigkdd international conference on*

- 748 *knowledge discovery and data mining* (pp. 2325–2335). Retrieved from
749 <http://arxiv.org/abs/1809.07394><https://arxiv.org/abs/1809.07394>
750 doi: 10.1145/3292500.3330674
- 751 Isaksen, L., Bonavita, M., Buizza, R., Fisher, M., Haseler, J., Leutbecher, M., &
752 Raynaud, L. (2010). Ensemble of data assimilations at ECMWF. *ECMWF*
753 *Tech. Memo.*, 636(December), 1–41.
- 754 Kingma, D. P., & Ba, J. (2014). Adam: A Method for Stochastic Optimization.
755 *ArXiv*. Retrieved from <http://arxiv.org/abs/1412.6980>
- 756 Larraondo, P. R., Renzullo, L. J., Inza, I., & Lozano, J. A. (2019). A data-driven
757 approach to precipitation parameterizations using convolutional encoder-
758 decoder neural networks. *ArXiv*. Retrieved from [http://arxiv.org/abs/](http://arxiv.org/abs/1903.10274)
759 [1903.10274](http://arxiv.org/abs/1903.10274)
- 760 Leutbecher, M. (2018, sep). Ensemble size: How suboptimal is less than infinity?
761 *Quarterly Journal of the Royal Meteorological Society*, 145(S1), 107–128. doi:
762 10.1002/qj.3387
- 763 Monhart, S., Spirig, C., Bhend, J., Bogner, K., Schär, C., & Liniger, M. A. (2018,
764 Aug). Skill of subseasonal forecasts in Europe: Effect of bias correction and
765 downscaling using surface observations. *Journal of Geophysical Research: At-*
766 *mospheres*. Retrieved from <http://doi.wiley.com/10.1029/2017JD027923>
767 doi: 10.1029/2017JD027923
- 768 Palmer, T. (2018). The ECMWF ensemble prediction system: Looking back (more
769 than) 25 years and projecting forward 25 years. *Quarterly Journal of the Royal*
770 *Meteorological Society*. Retrieved from [http://doi.wiley.com/10.1002/qj](http://doi.wiley.com/10.1002/qj.3383)
771 [.3383](http://doi.wiley.com/10.1002/qj.3383) doi: 10.1002/qj.3383
- 772 Richardson, D. S. (2000). Skill and relative economic value of the ECMWF ensem-
773 ble prediction system. *Quarterly Journal of the Royal Meteorological Society*,
774 126(563), 649–667. doi: <https://doi.org/10.1002/qj.49712656313>
- 775 Ronneberger, O., Fischer, P., & Brox, T. (2015). U-net: Convolutional networks
776 for biomedical image segmentation. In *Lecture notes in computer science (in-*
777 *cluding subseries lecture notes in artificial intelligence and lecture notes in*
778 *bioinformatics)* (Vol. 9351, pp. 234–241). Springer, Cham. Retrieved from
779 [http://link.springer.com/10.1007/978-3-319-24574-4{ }28](http://link.springer.com/10.1007/978-3-319-24574-4_{ }28) doi:
780 10.1007/978-3-319-24574-4_28
- 781 Scher, S., & Messori, G. (2019). Weather and climate forecasting with neu-
782 ral networks: using GCMs with different complexity as study-ground.
783 *Geoscientific Model Development Discussions*(March), 1–15. Retrieved
784 from <https://www.geosci-model-dev-discuss.net/gmd-2019-53/>
785 [{\%}0Ahttps://www.geosci-model-dev-discuss.net/gmd-2019-53/](https://www.geosci-model-dev-discuss.net/gmd-2019-53/) doi:
786 10.5194/gmd-2019-53
- 787 Scher, S., & Messori, G. (2020, feb). Ensemble neural network forecasts with singu-
788 lar value decomposition. *ArXiv*. Retrieved from [http://arxiv.org/abs/2002](http://arxiv.org/abs/2002.05398)
789 [.05398](http://arxiv.org/abs/2002.05398)
- 790 Toms, B. A., Barnes, E. A., & Ebert-Uphoff, I. (2020). Physically Interpretable Neu-
791 ral Networks for the Geosciences: Applications to Earth System Variability.
792 *Journal of Advances in Modeling Earth Systems*, 12(9), e2019MS002002. doi:
793 10.1029/2019MS002002
- 794 Ullrich, P. A., Devendran, D., & Johansen, H. (2016). Arbitrary-order conserva-
795 tive and consistent remapping and a theory of linear maps: Part II. *Monthly*
796 *Weather Review*, 144(4), 1529–1549. doi: 10.1175/MWR-D-15-0301.1
- 797 Ullrich, P. A., & Taylor, M. A. (2015). Arbitrary-order conservative and consis-
798 tent remapping and a theory of linear maps: Part I. *Monthly Weather Review*,
799 143(6), 2419–2440. doi: 10.1175/MWR-D-14-00343.1
- 800 Vitart, F. (2004). Monthly forecasting at ECMWF. *Monthly Weather Review*,
801 132(12), 2761–2779. doi: 10.1175/MWR2826.1
- 802 Vitart, F. (2014). Evolution of ECMWF sub-seasonal forecast skill scores. *Quar-*

- 803 *terly Journal of the Royal Meteorological Society*, 140(683), 1889–1899. doi: 10
804 .1002/qj.2256
- 805 Vitart, F., Ardilouze, C., Bonet, A., Brookshaw, A., Chen, M., Codorean, C., ...
806 Zhang, L. (2017). The Subseasonal to Seasonal (S2S) Prediction Project
807 Database. *Bulletin of the American Meteorological Society*, 98(1), 163–173.
808 doi: 10.1175/BAMS-D-16-0017.1
- 809 Weigel, A. P., Baggenstos, D., Liniger, M. A., Vitart, F., & Appenzeller, C.
810 (2008, dec). Probabilistic Verification of Monthly Temperature Fore-
811 casts. *Monthly Weather Review*, 136(12), 5162–5182. Retrieved from
812 <http://journals.ametsoc.org/doi/10.1175/2008MWR2551.1> doi:
813 10.1175/2008MWR2551.1
- 814 Weigel, A. P., Liniger, M. A., & Appenzeller, C. (2007, jan). The discrete Brier and
815 ranked probability skill scores. *Monthly Weather Review*, 135(1), 118–124. Re-
816 trieved from <http://journals.ametsoc.org/doi/10.1175/MWR3280.1> doi:
817 10.1175/MWR3280.1
- 818 Weyn, J. A., Durran, D. R., & Caruana, R. (2019). Can Machines Learn to Pre-
819 dict Weather? Using Deep Learning to Predict Gridded 500-hPa Geopotential
820 Height From Historical Weather Data. *Journal of Advances in Modeling Earth*
821 *Systems*, 11(8), 2680–2693. doi: 10.1029/2019ms001705
- 822 Weyn, J. A., Durran, D. R., & Caruana, R. (2020). Improving data-driven
823 global weather prediction using deep convolutional neural networks on a
824 cubed sphere. *Journal of Advances in Modeling Earth Systems*, 12(9),
825 e2020MS002109. doi: 10.1029/2020MS002109
- 826 White, C. J., Carlsen, H., Robertson, A. W., Klein, R. J. T., Lazo, J. K., Ku-
827 mar, A., ... Zebiak, S. E. (2017). Potential applications of subseasonal-to-
828 seasonal (S2S) predictions. *Meteorological Applications*, 24(3), 315–325. doi:
829 10.1002/met.1654

Figure 1.

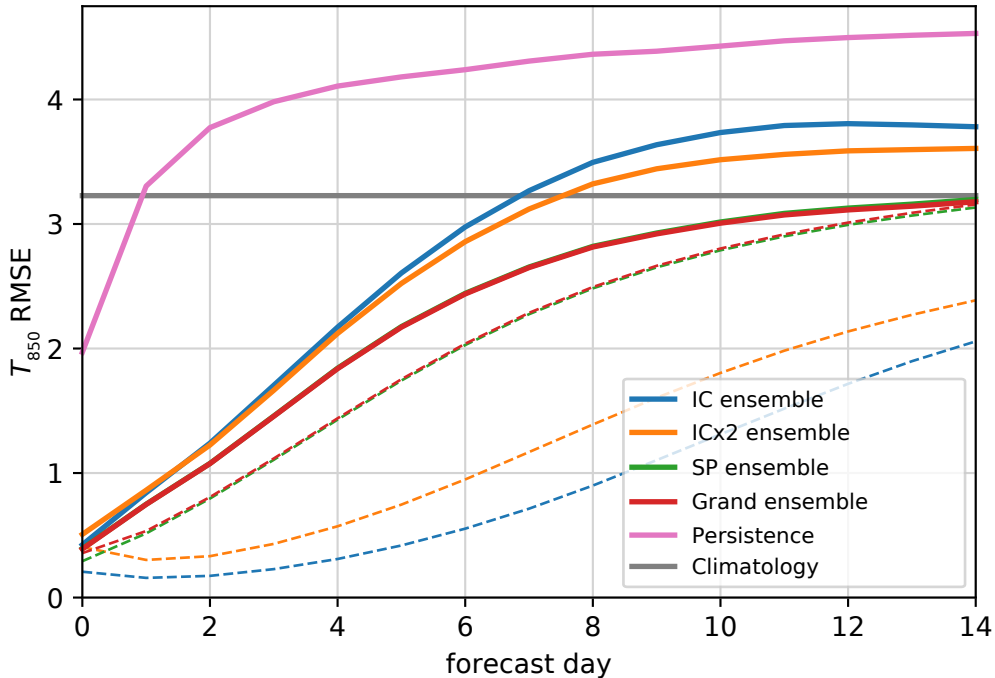


Figure 2.

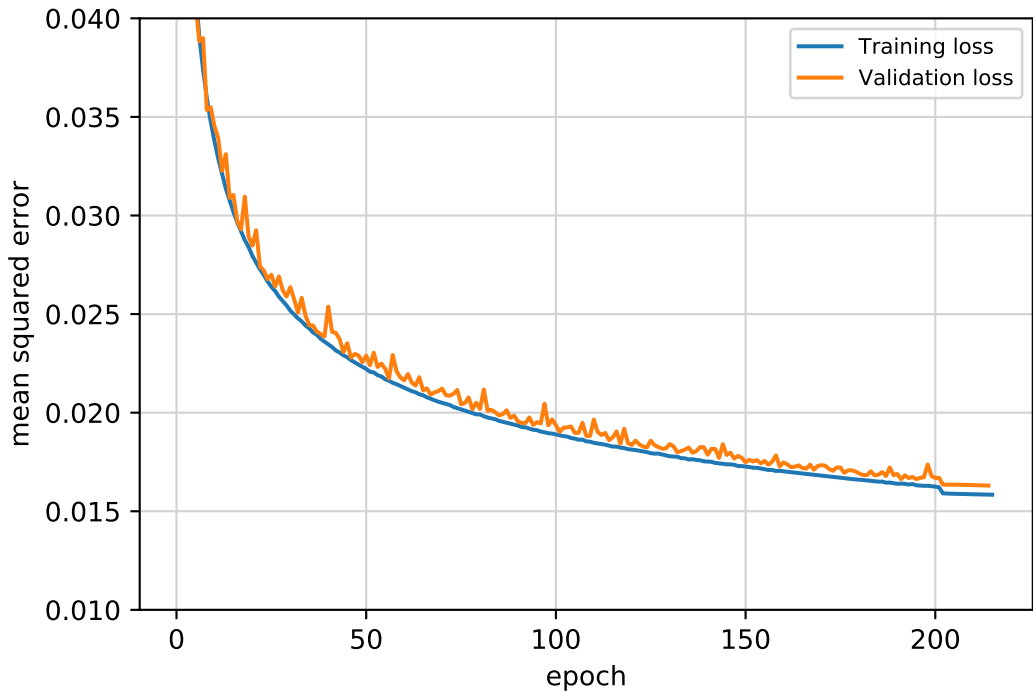
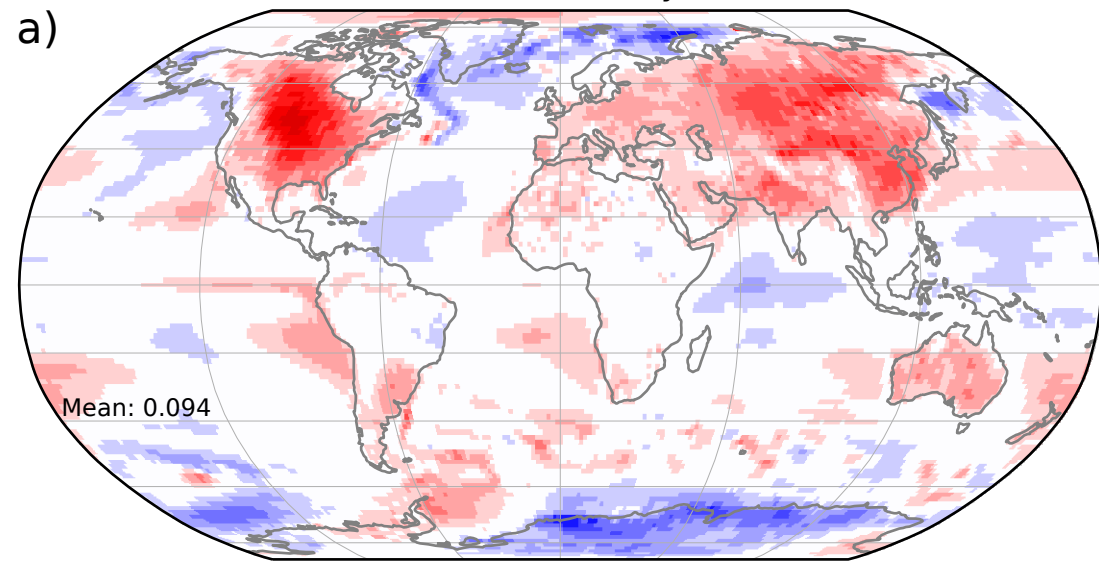
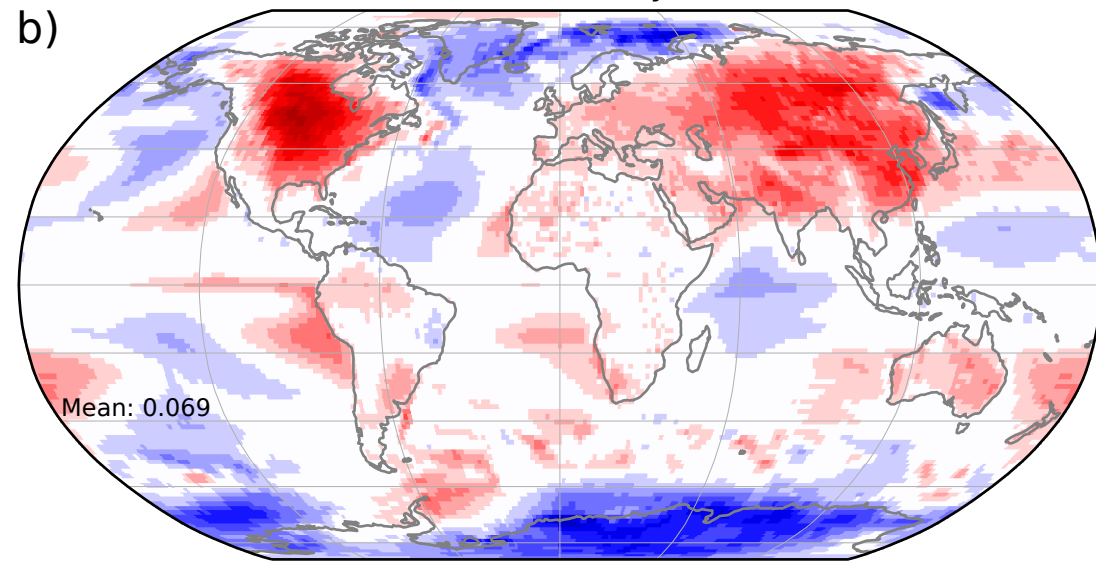


Figure 3.

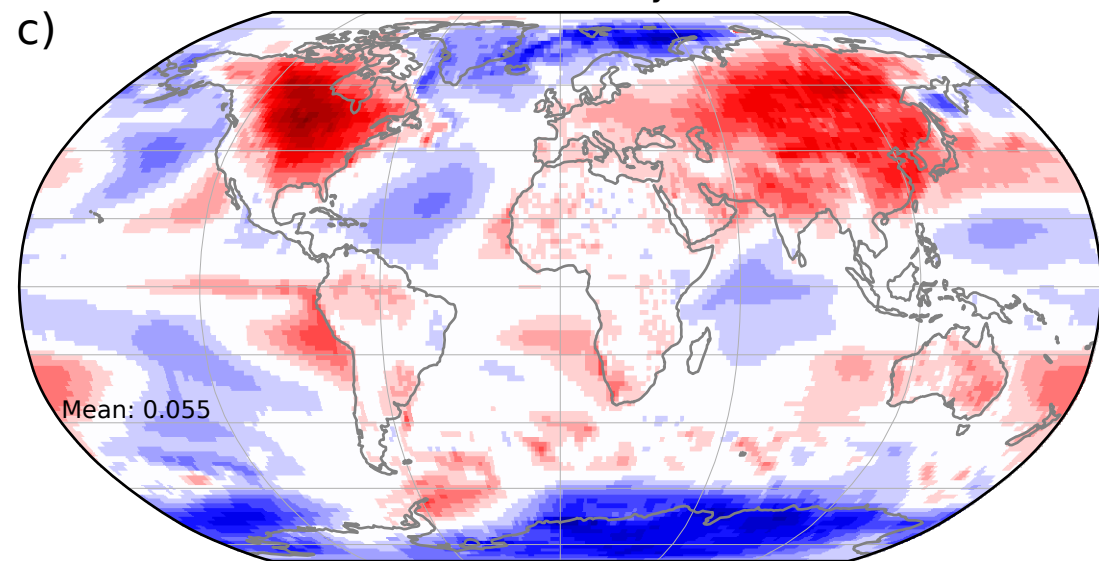
DLWP ensemble, days 8-14



DLWP ensemble, days 15-21



DLWP ensemble, days 22-28



DLWP ensemble, days 29-42

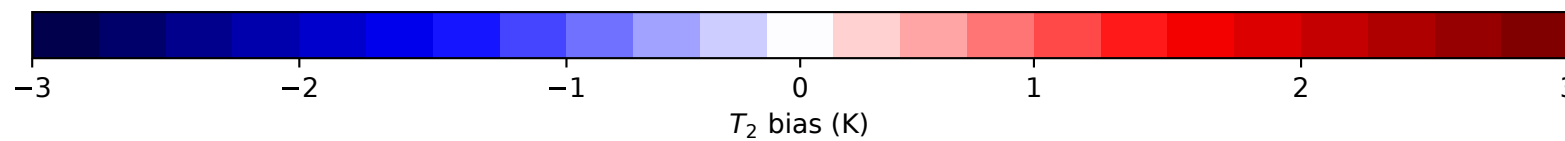
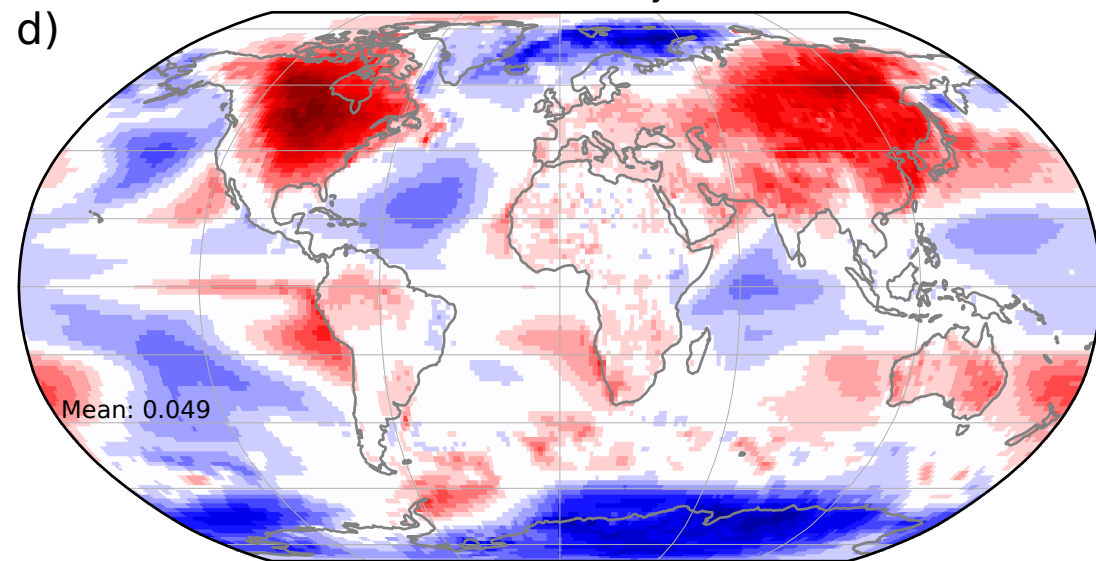


Figure 4.

(a) Forecast

(b) Verification

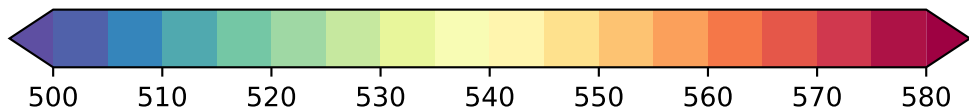
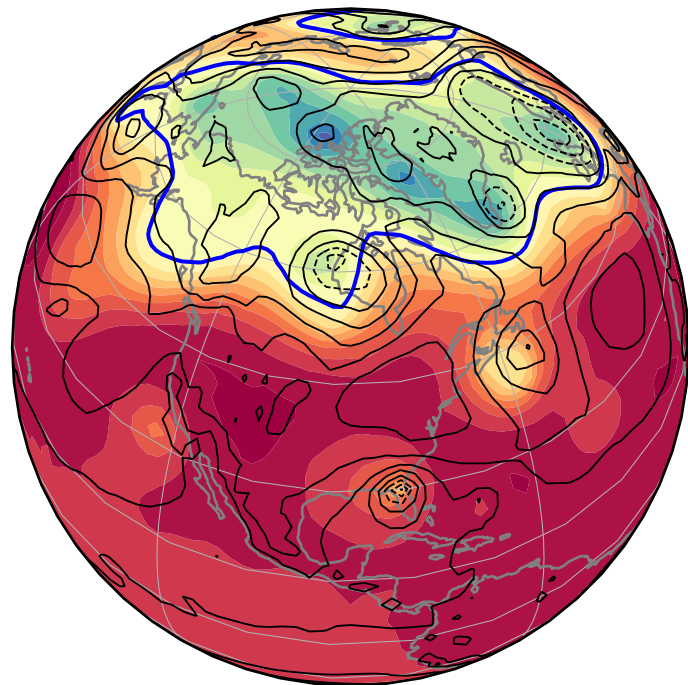
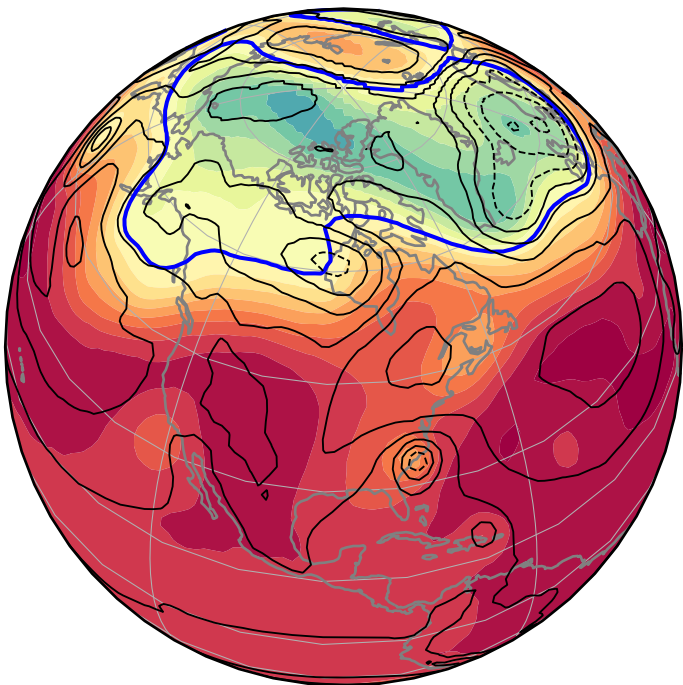


Figure 5.

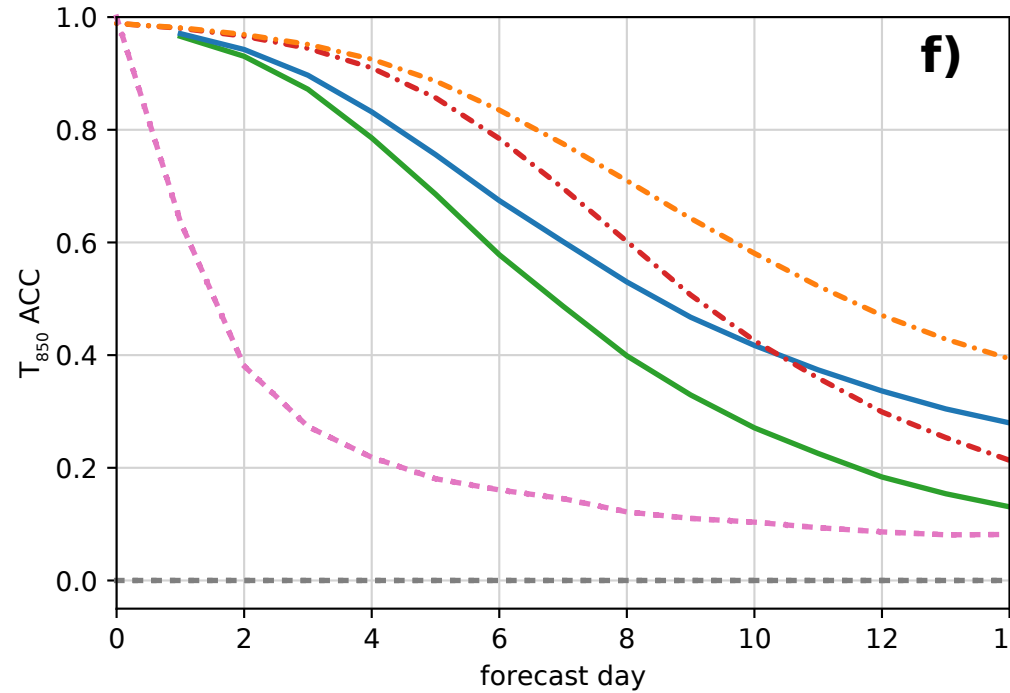
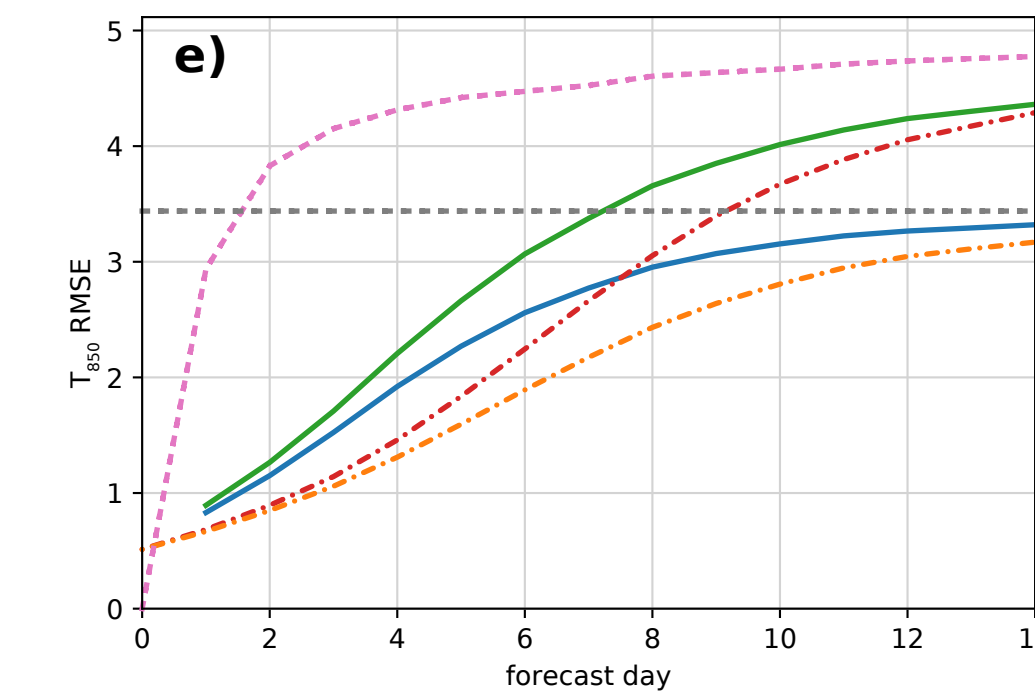
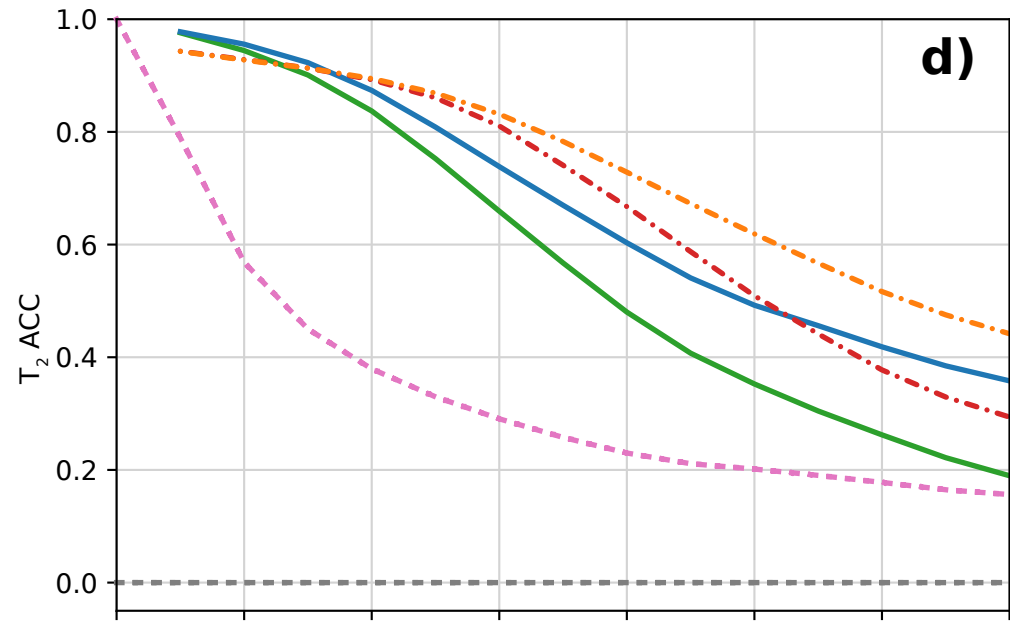
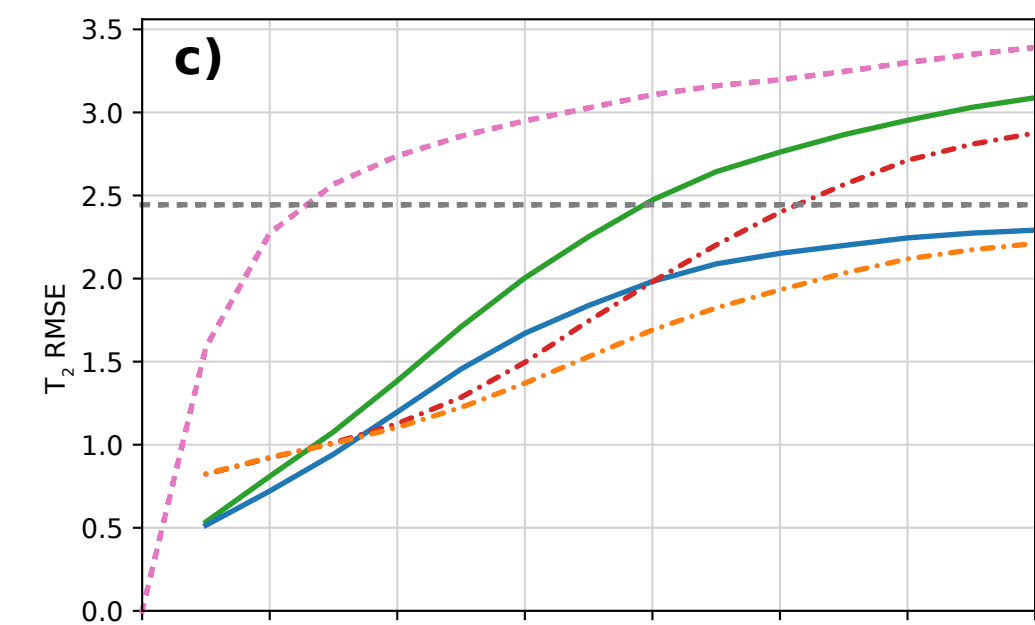
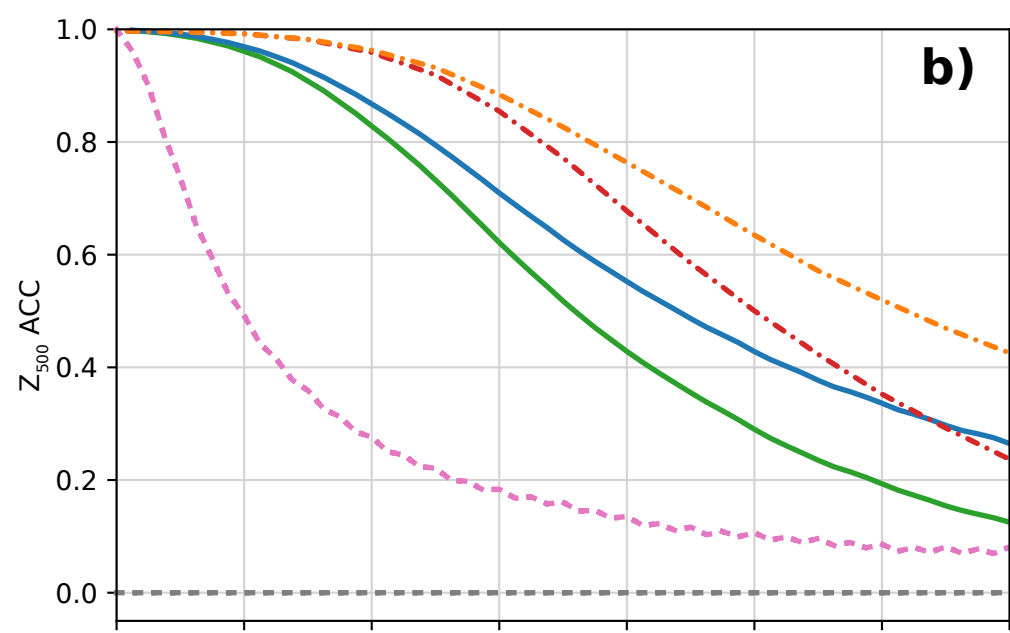
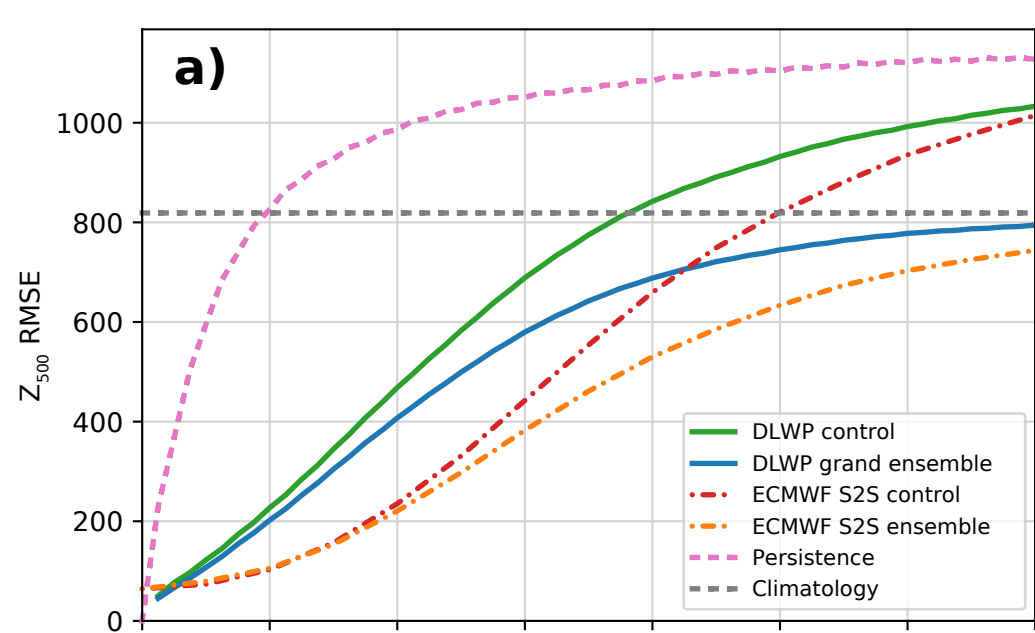
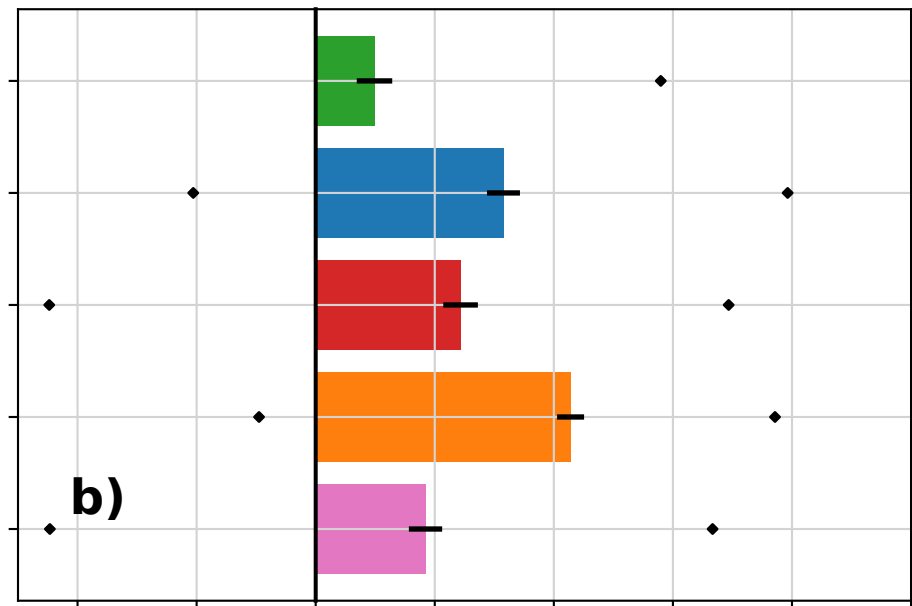
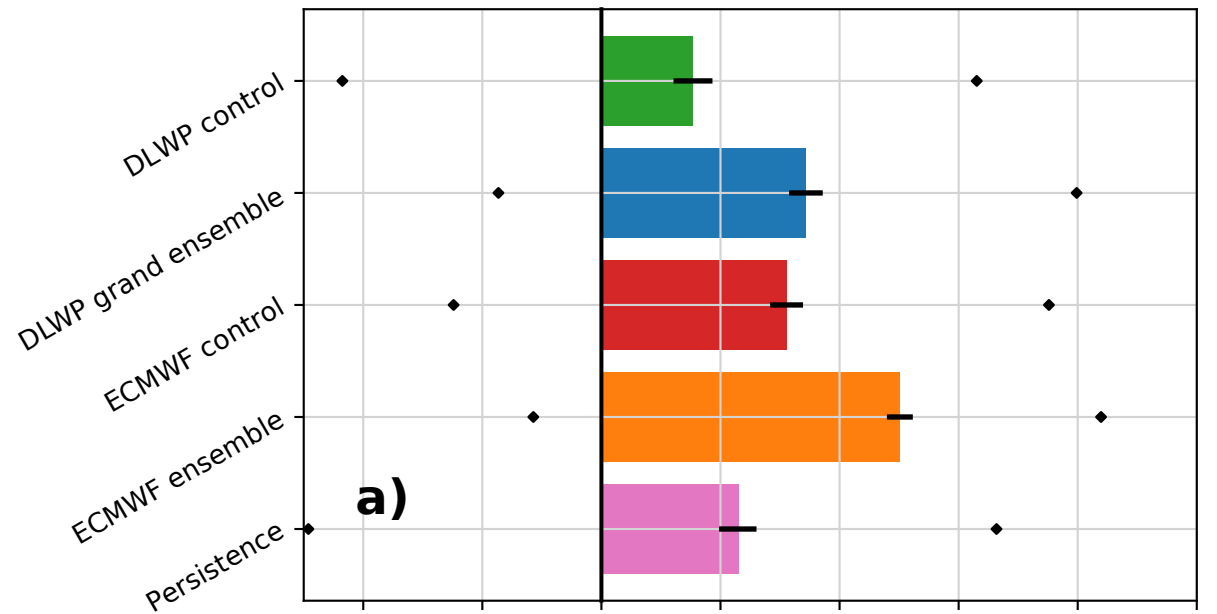


Figure 6.

2-m Temperature

Weeks 3-4

Weeks 5-6



T₈₅₀

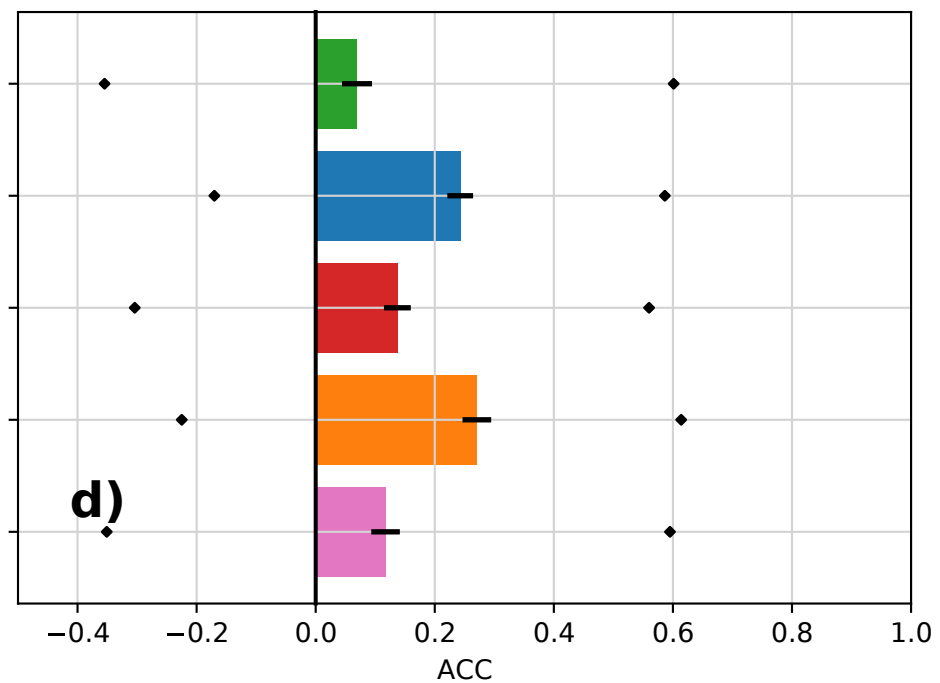
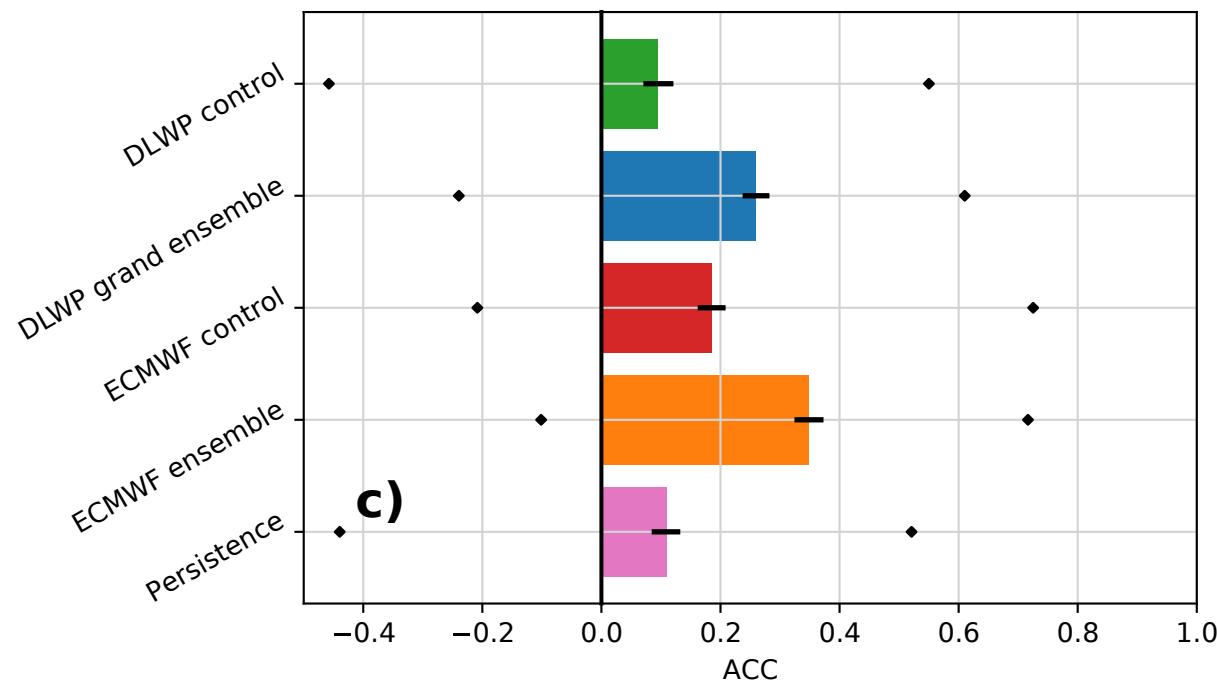
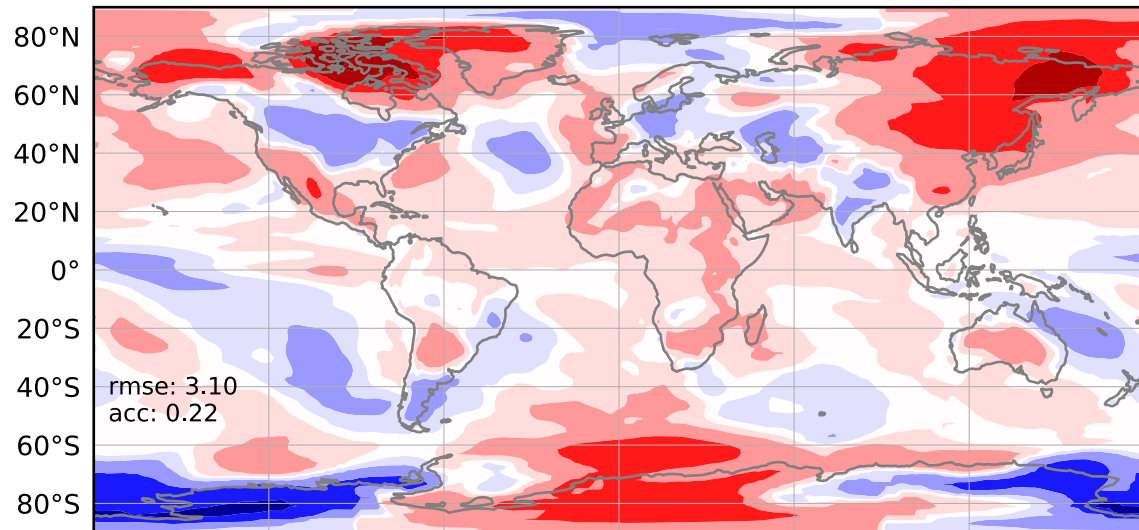
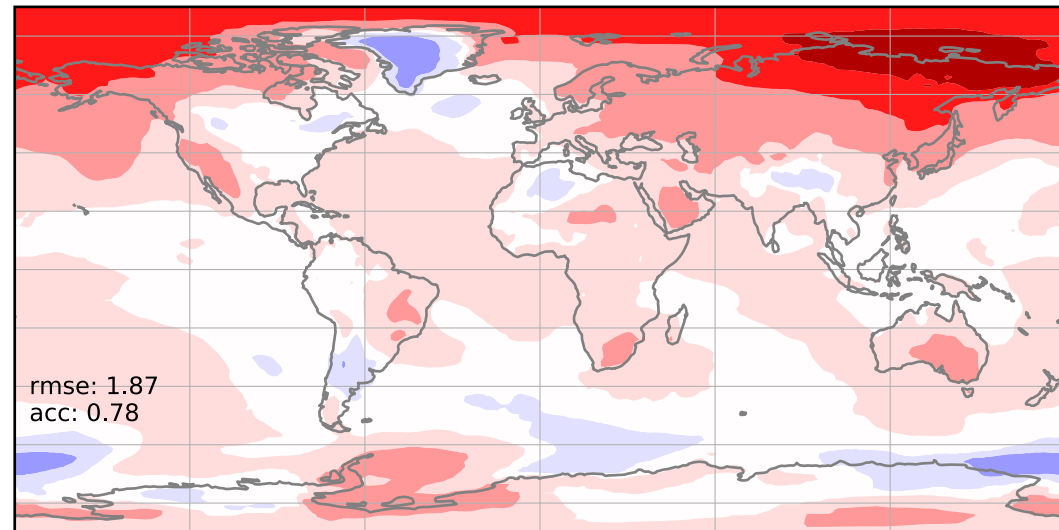


Figure 7.

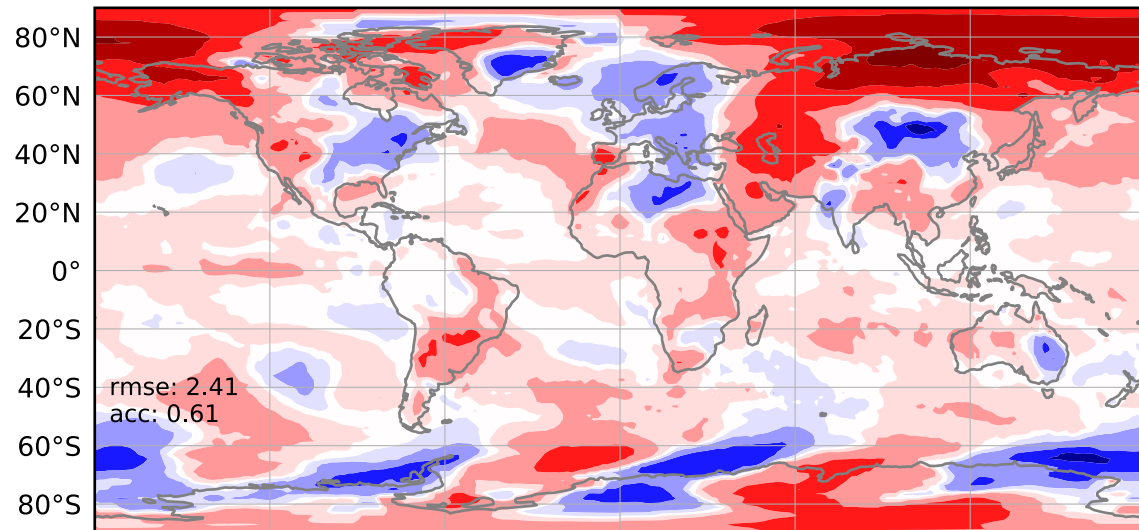
(a) DLWP Control



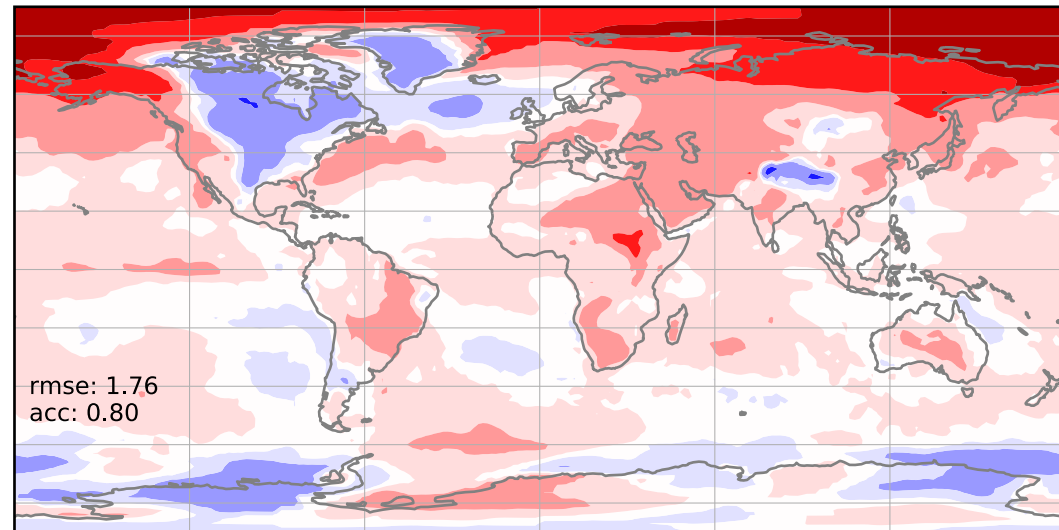
(b) DLWP Ensemble



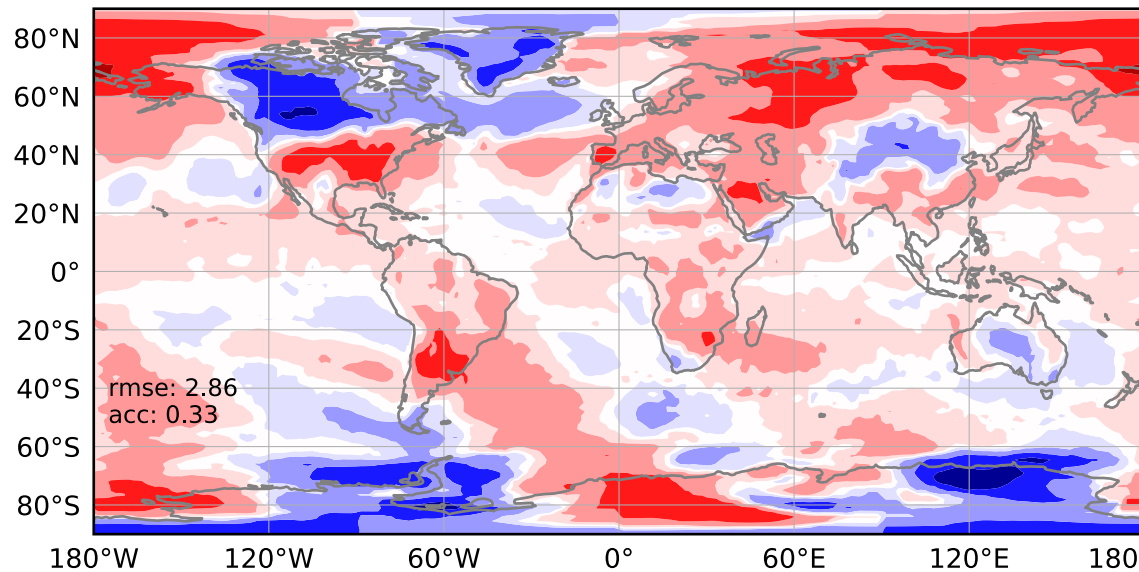
(c) ECMWF Control



(d) ECMWF Ensemble



(e) Persistence



(f) Verification

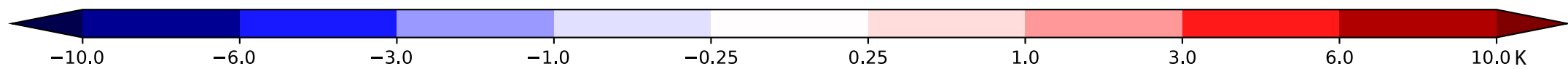
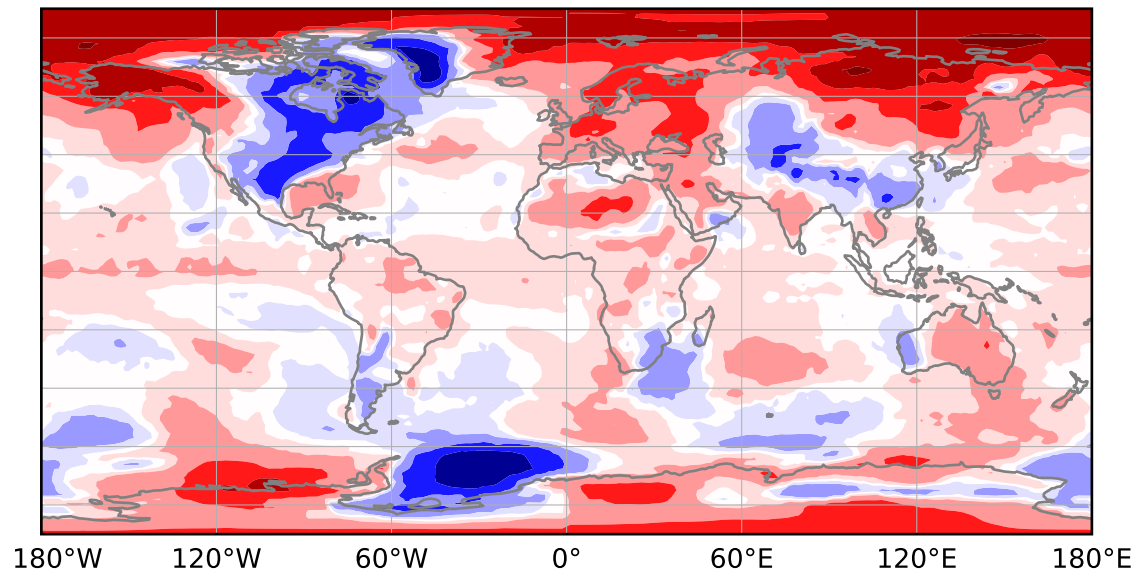


Figure 8.

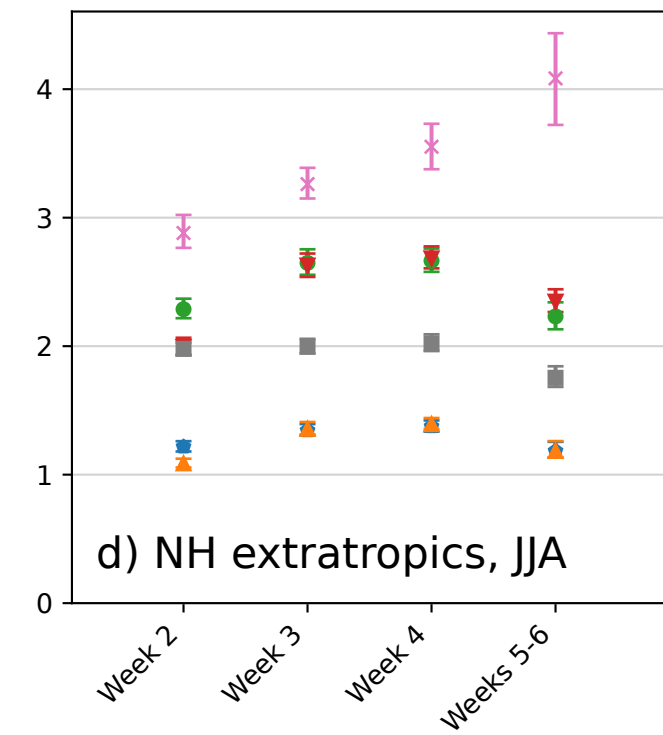
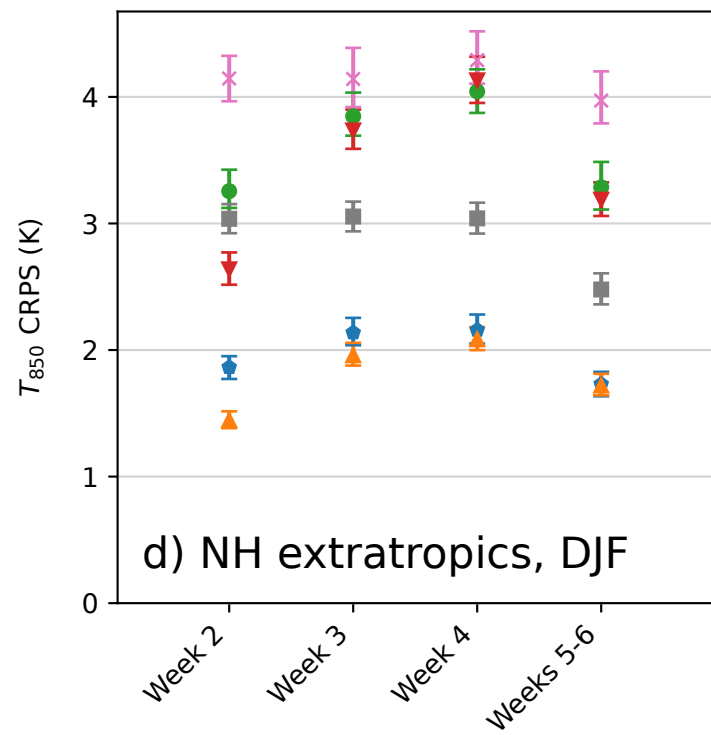
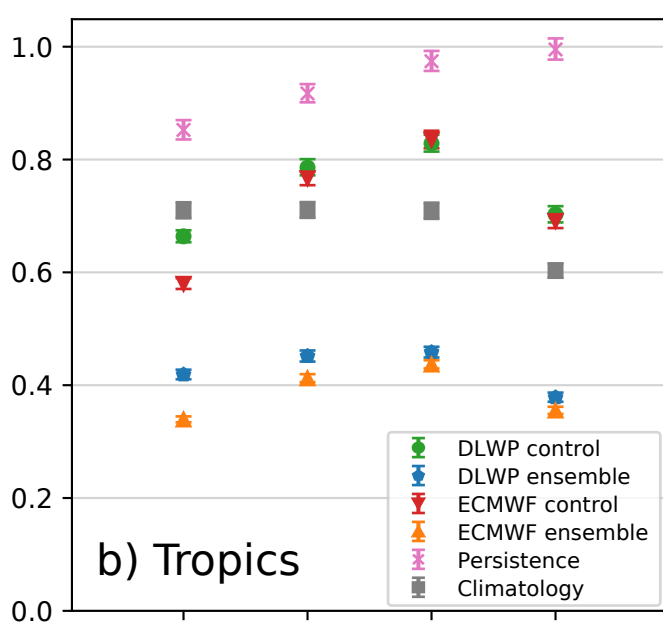
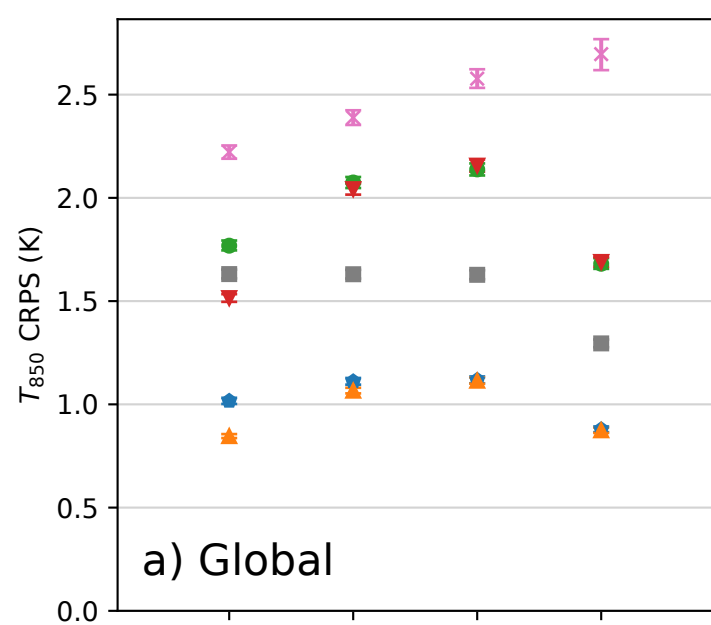


Figure 9.

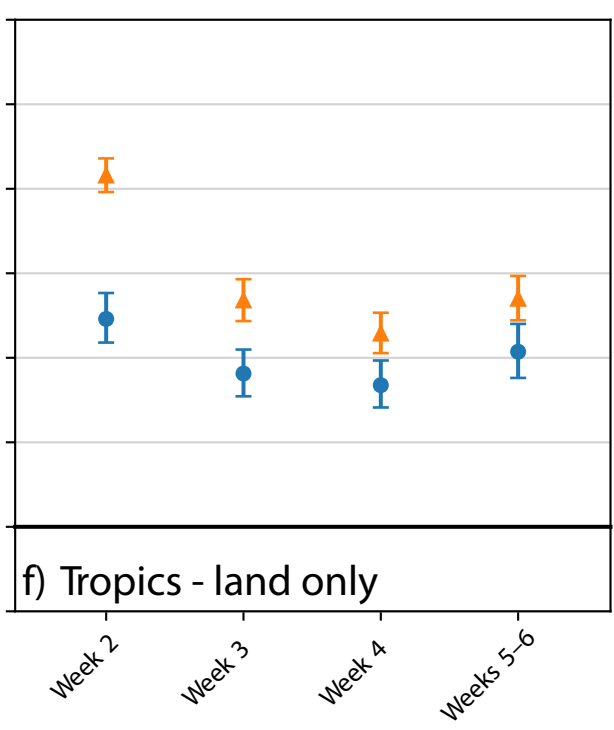
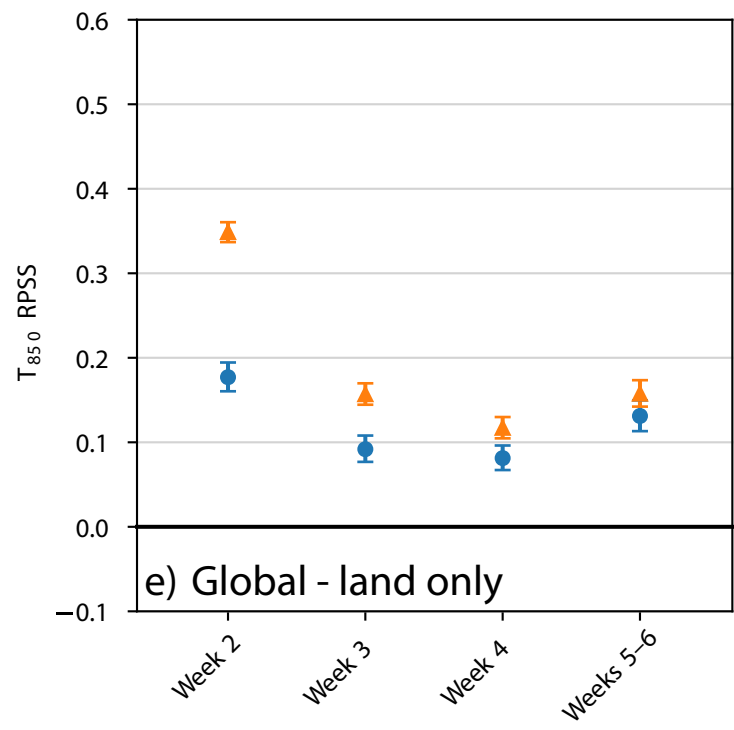
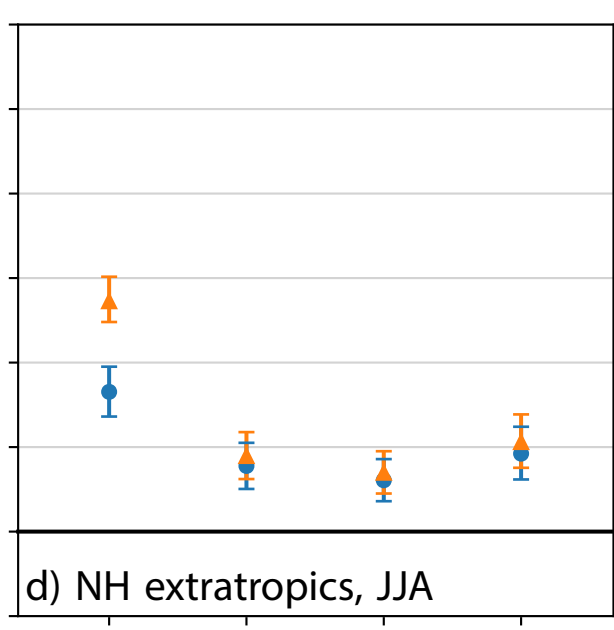
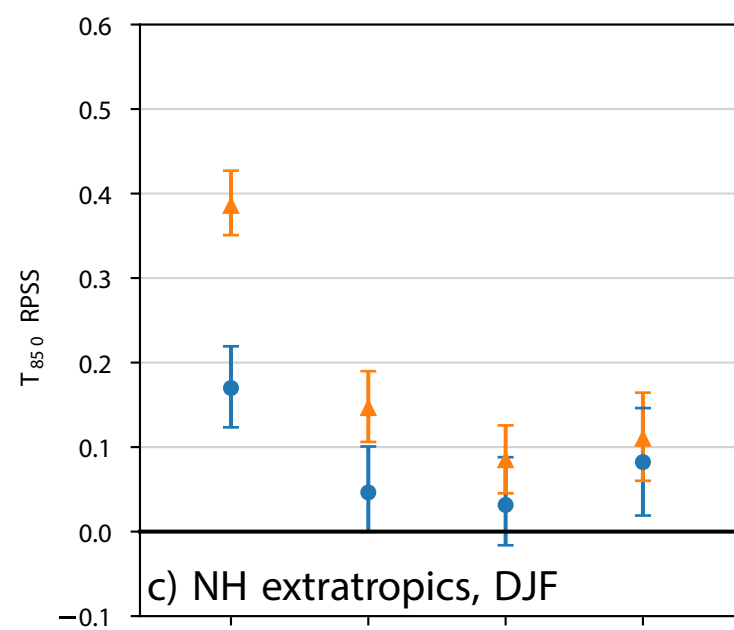
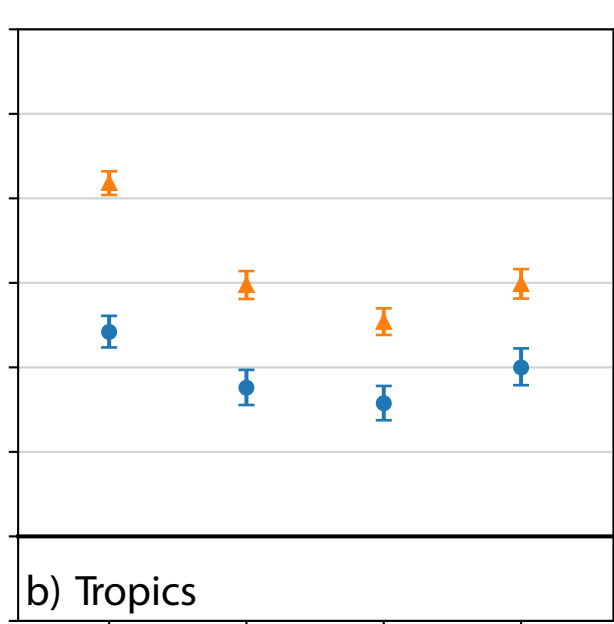
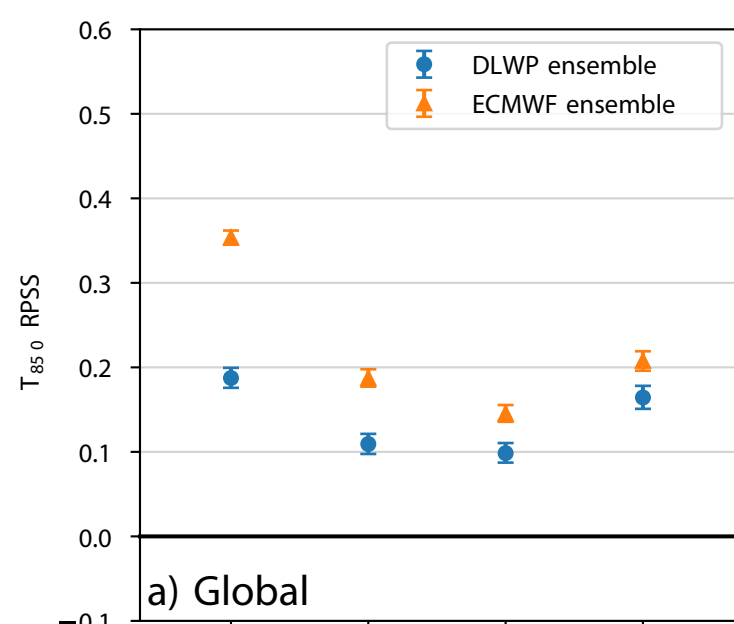


Figure 10.

DLWP ensemble

ECMWF ensemble

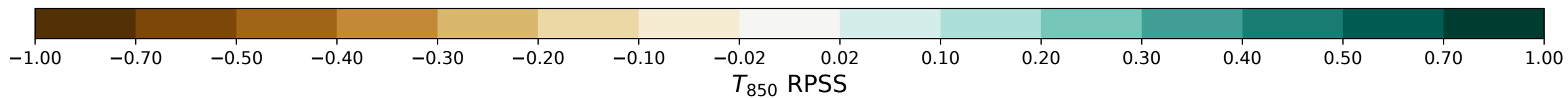
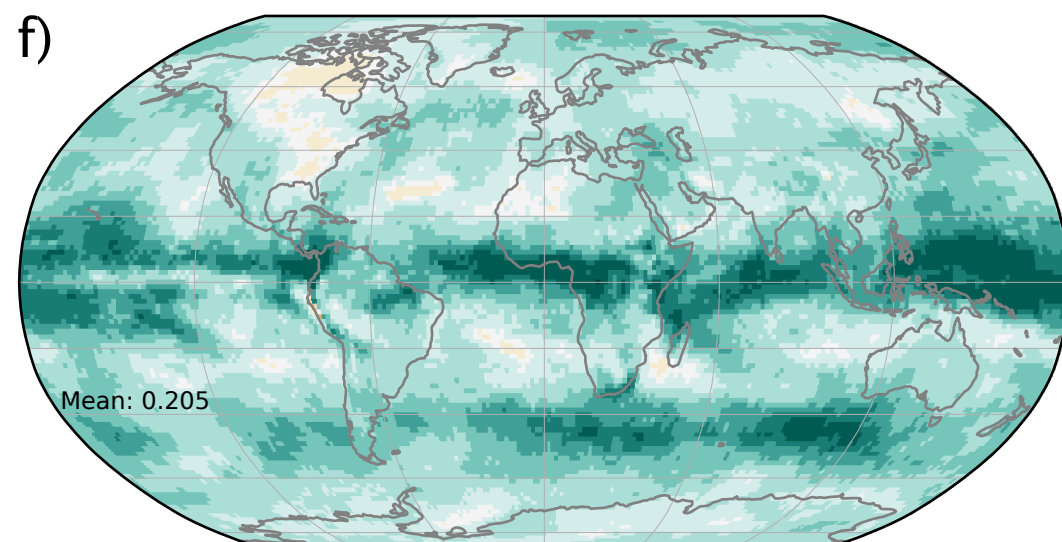
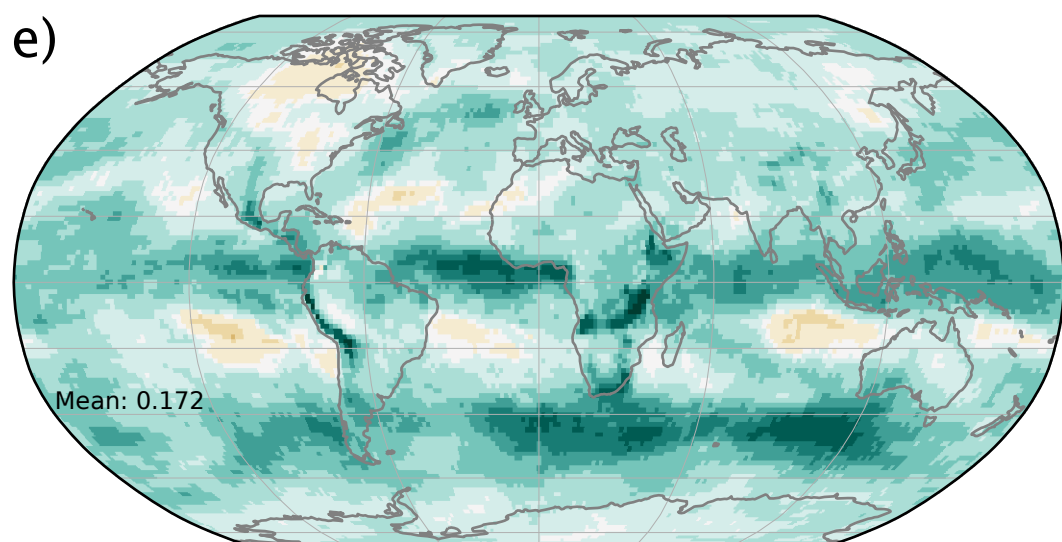
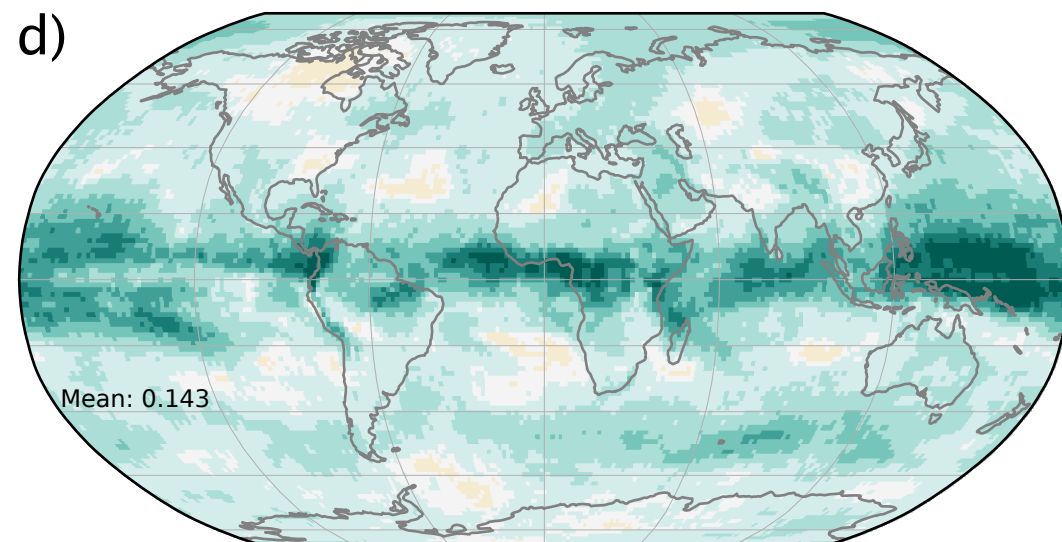
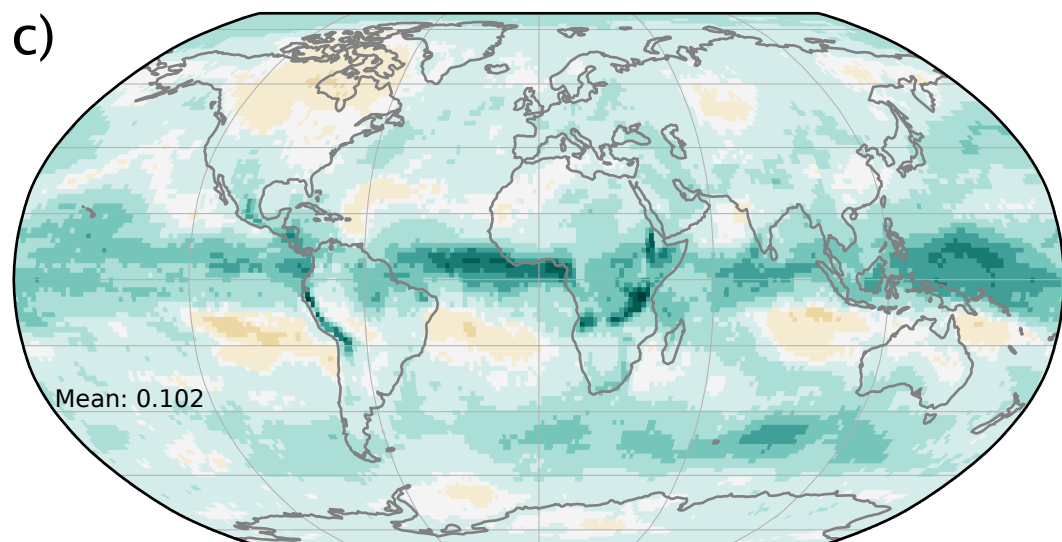
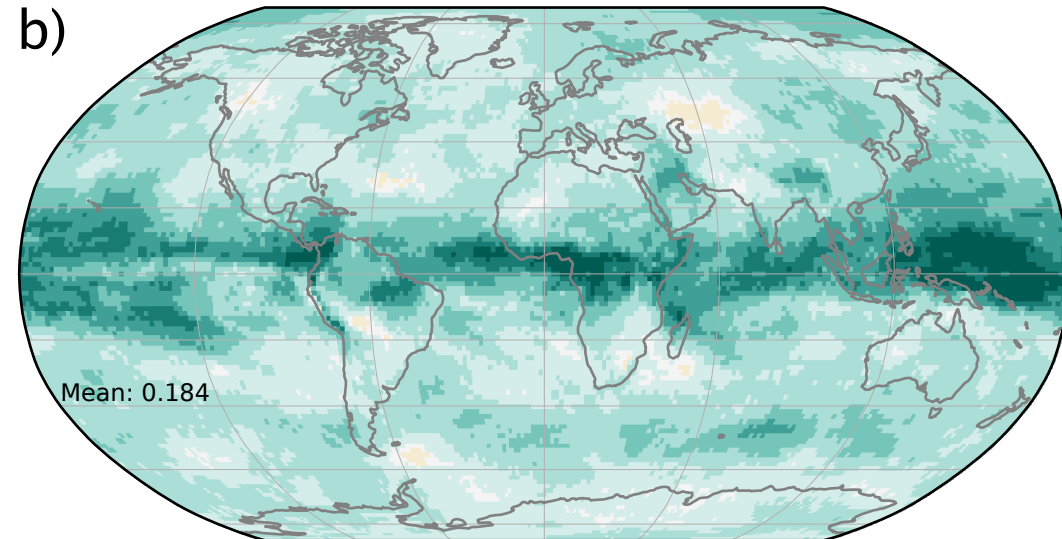
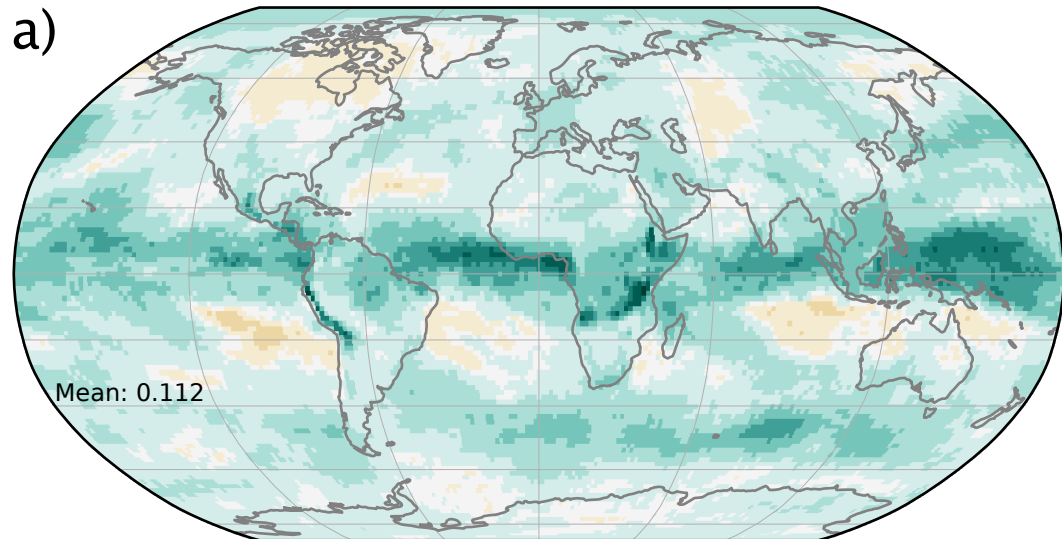


Figure 11.

DLWP ensemble

ECMWF ensemble

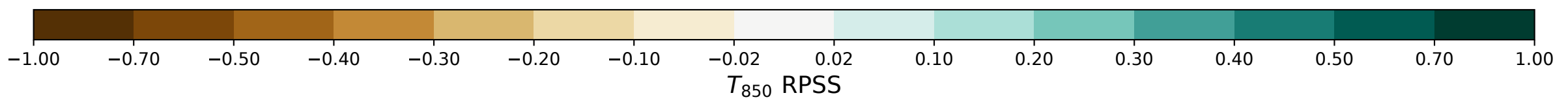
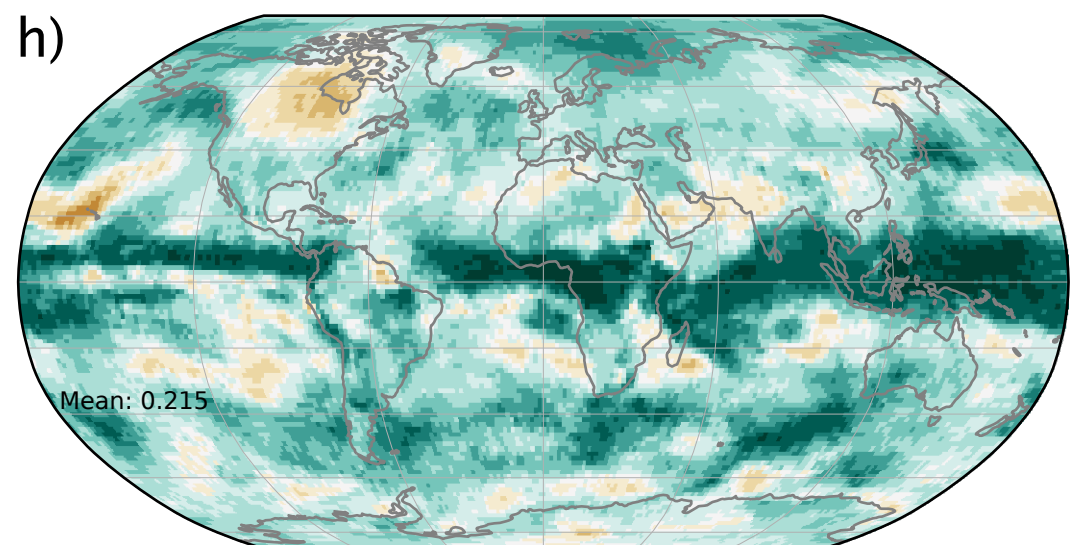
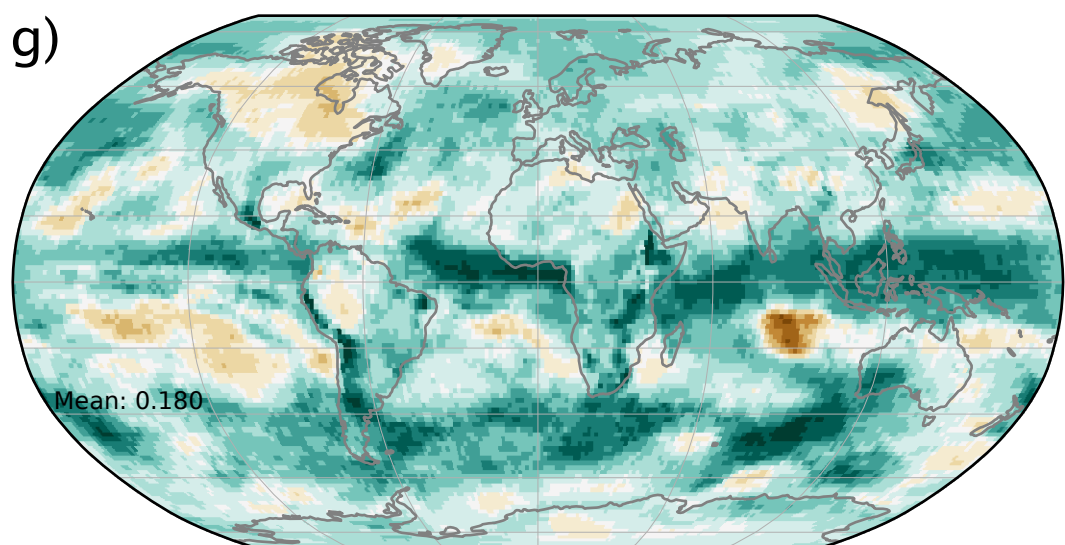
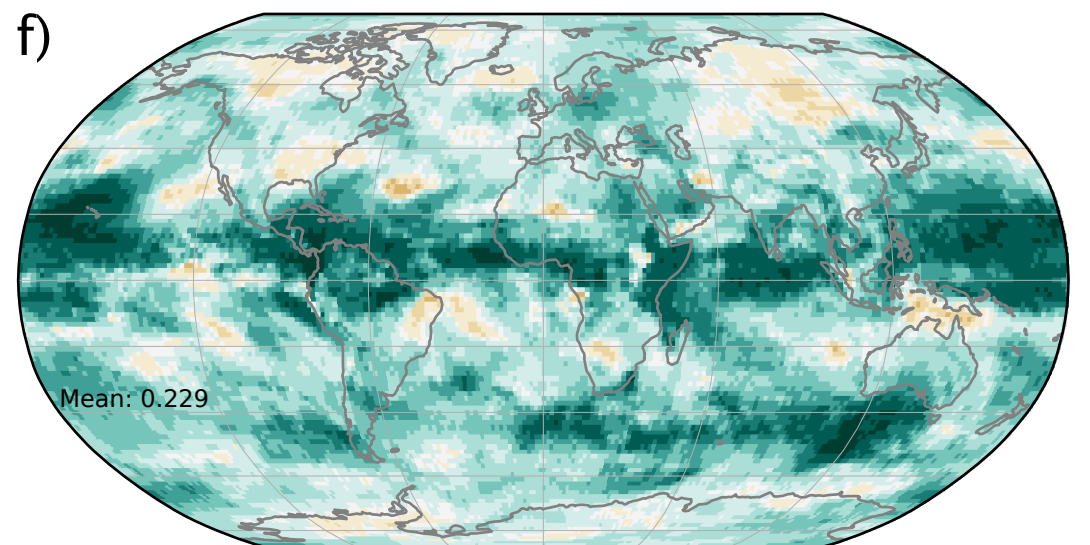
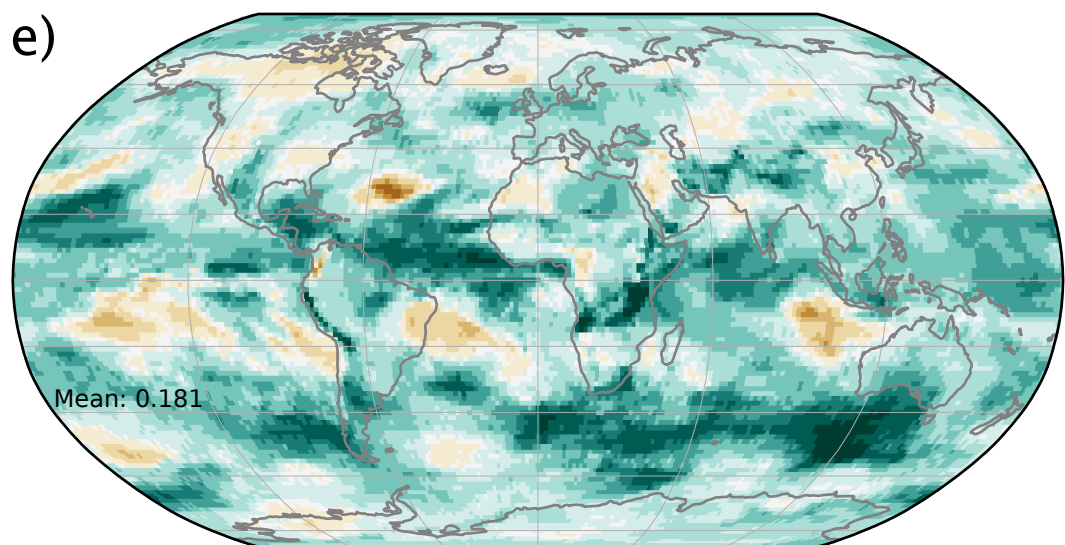
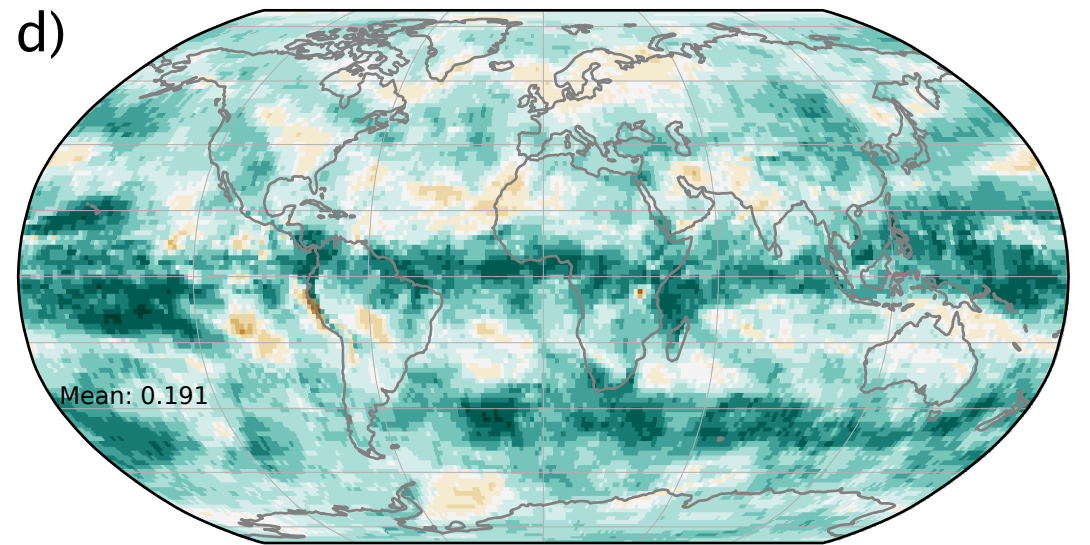
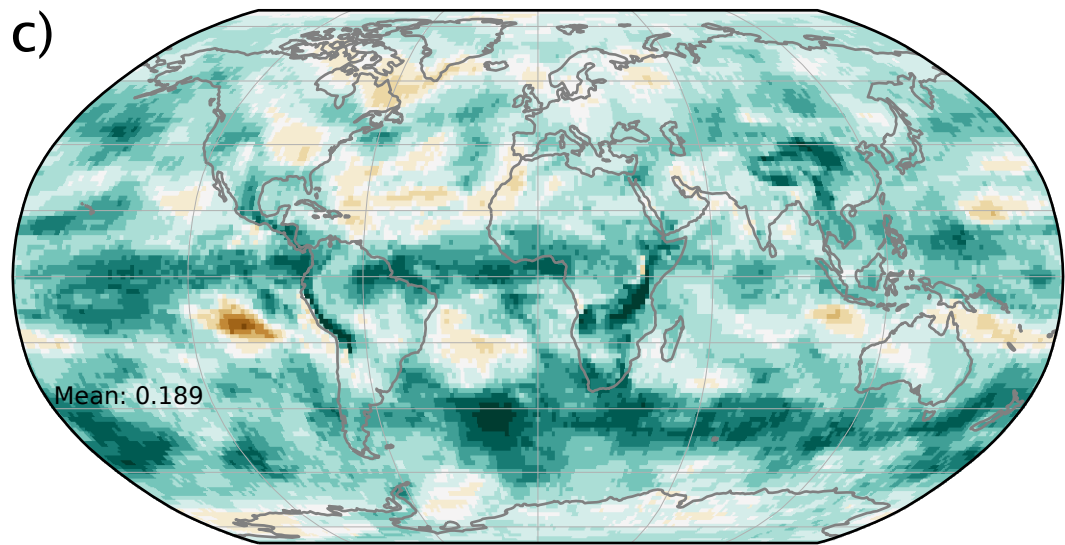
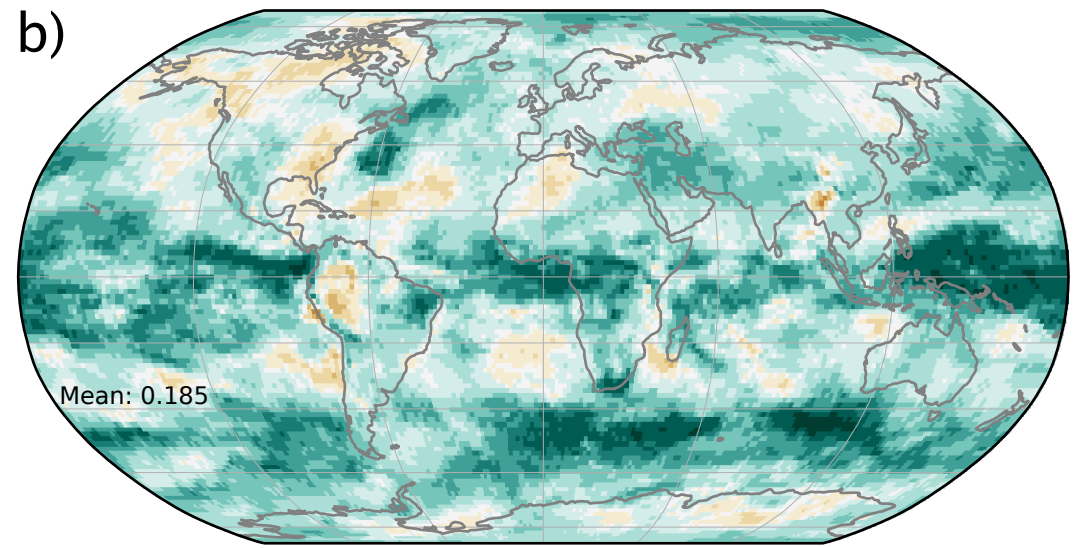
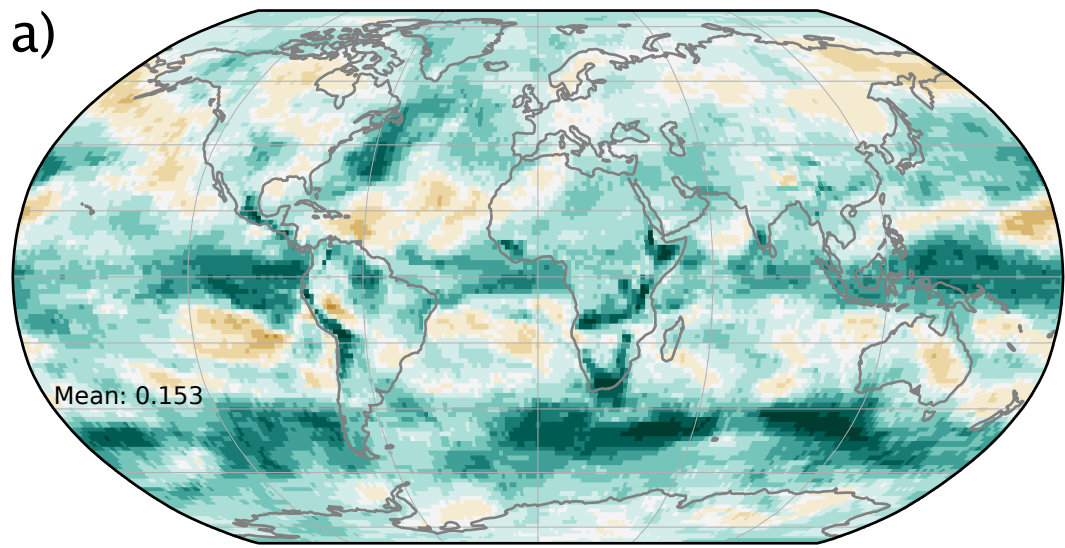


Figure 12.

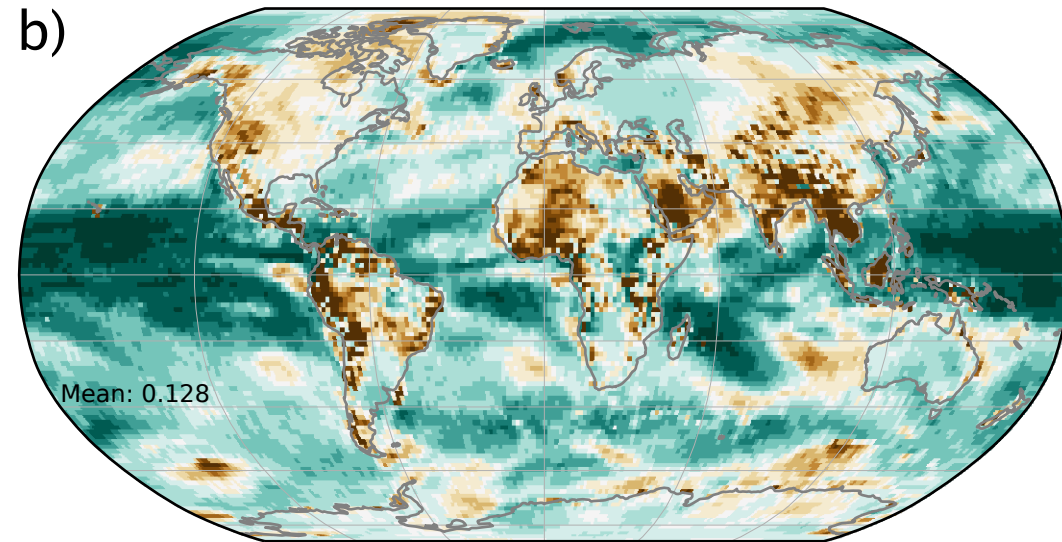
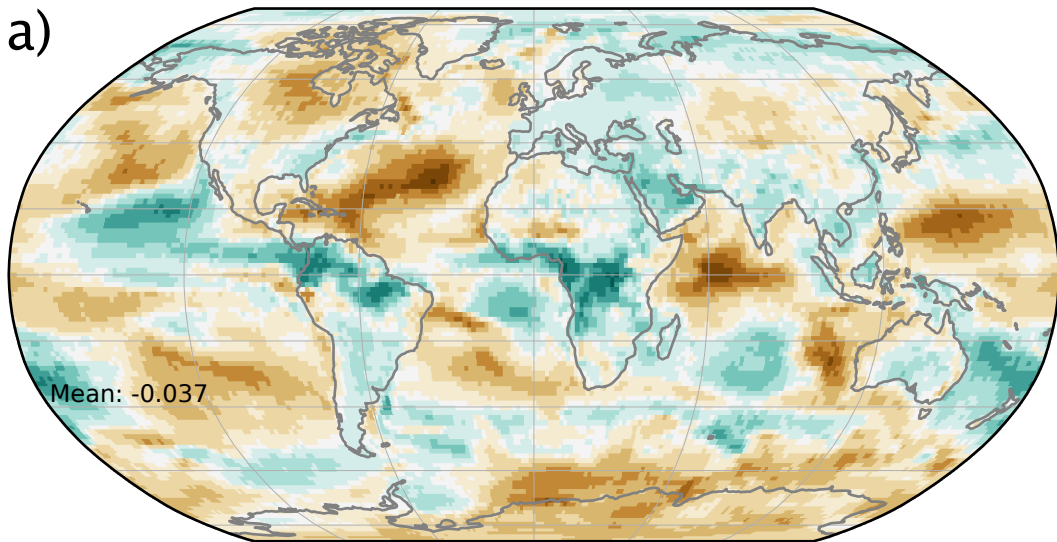
DLWP ensemble

ECMWF ensemble

a)

b)

Uncorrected



c)

d)

Bias-corrected

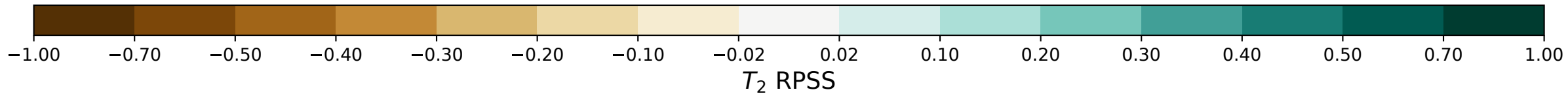
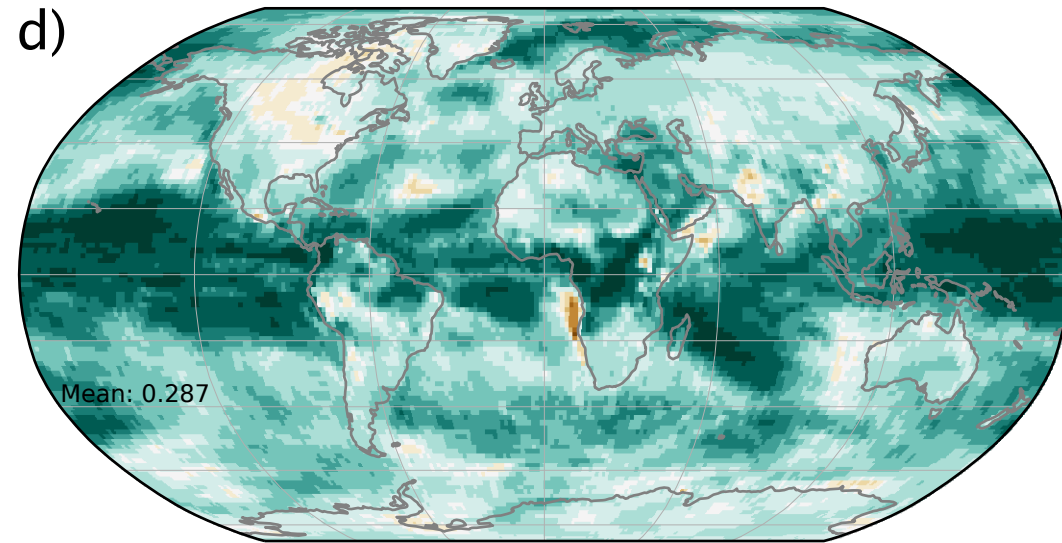
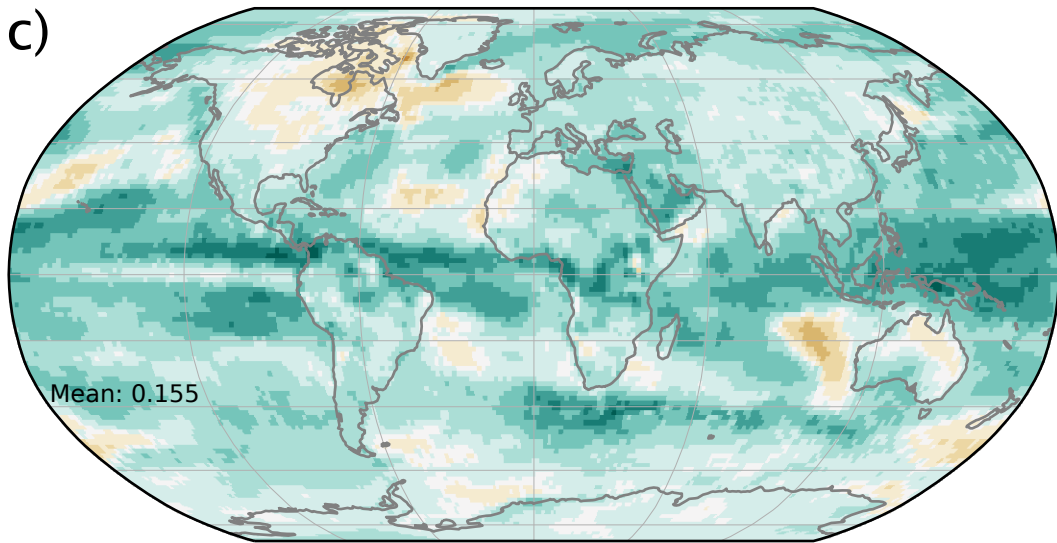
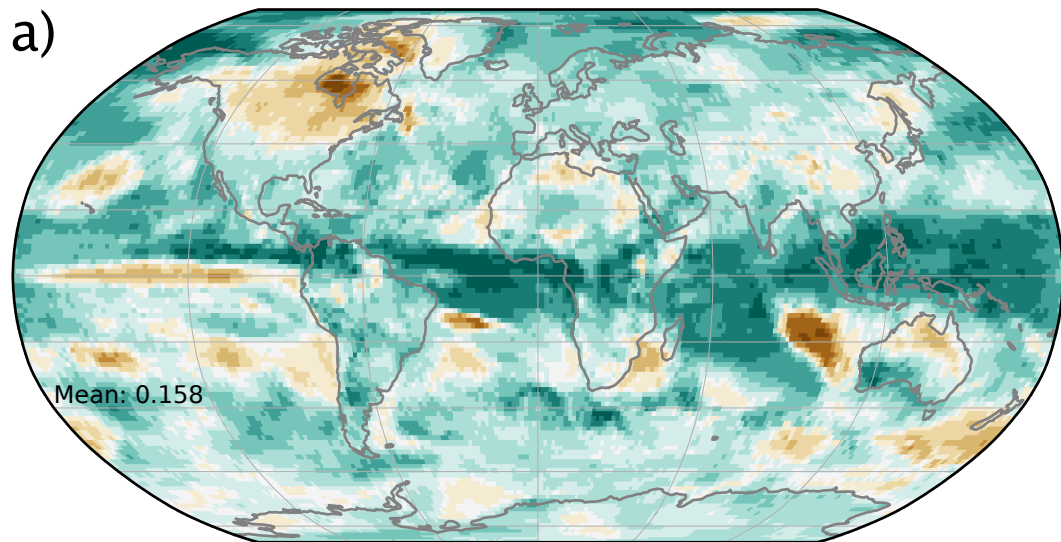


Figure 13.

DLWP ensemble

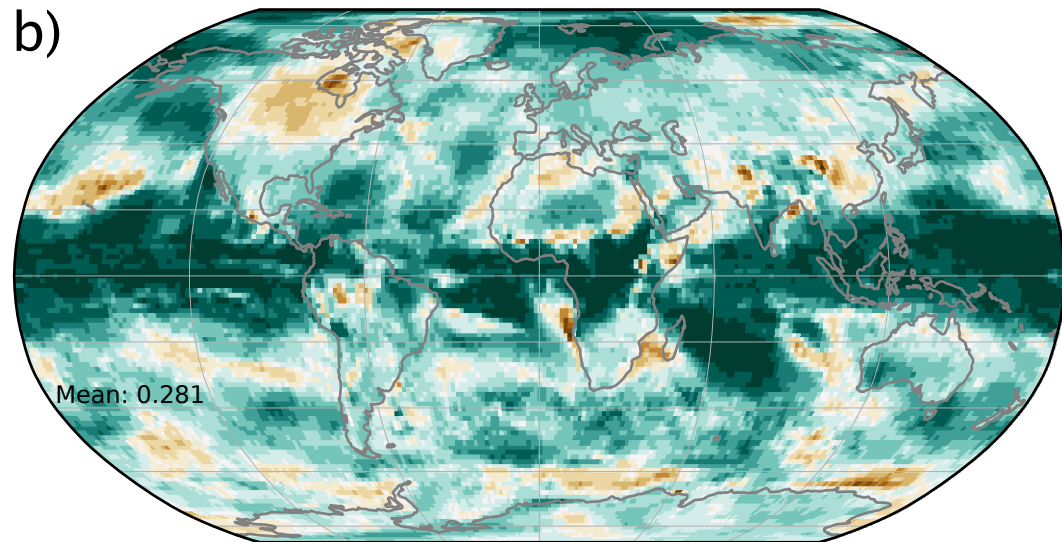
a)



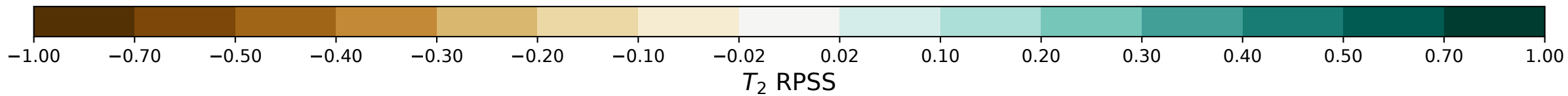
Mean: 0.158

ECMWF ensemble

b)



Mean: 0.281



T_2 RPSS